UNIVERSITÉ DE MONTRÉAL

SIX-PORT TECHNOLOGY FOR MILLIMETER-WAVE MIMO SYSTEMS

TAO JIANG

DÉPARTEMENT DE GÉNIE ÉLECTRIQUE

ÉCOLE POLYTECHNIQUE DE MONTRÉAL

MÉMOIRE PRÉSENTÉ EN VUE DE L'OBTENTION

DU DIPLÔME DE MAÎTRISE ÈS SCIENCES APPLIQUÉES

(GÉNIE ÉLECTRIQUE)

MAI 2014

UNIVERSITÉ DE MONTRÉAL

ÉCOLE POLYTECHNIQUE DE MONTRÉAL

Ce mémoire intitulé:

SIX-PORT TECHNOLOGY FOR MILLIMETER-WAVE MIMO SYSTEMS

présenté par : JIANG Tao

en vue de l'obtention du diplôme de : Maîtrise ès sciences appliquées

a été dûment accepté par le jury d'examen constitué de :

M. CARDINAL Christian, Ph.D., président

M. WU Ke, Ph.D., membre et directeur de recherche

M. TATU Serioja, Ph.D., membre et codirecteur de recherche

M. BOUTAYEB Halim, Ph.D., membre

DEDICATION

To my family

ACKNOWLEDGE

First of all, I would like to express my gratitude to my supervisor Dr. Ke Wu and co-supervisor Dr. Serioja Tatu, who gave me the opportunity to pursue the master studies at École Polytechnique de Montréal. Their passion for research, their patience, and their innovative ideas have impressed me and driven me to explore new space in our field and accomplish this thesis.

I would also like to thank all the personnels at the Poly-Grames Research Center, in particular the technician team including Mr. Jules Gauthier, Mr. Steve Dubé, Mr. Maxime Thibault, and Mr. Traian Antonescu, for their great work in circuit fabrication and measurement. My gratitude is extended to Mrs. Ginette Desparois and Mrs. Elena Pavlov for their administrative work and to Mr. Jean-Sébastien Décarie for his IT support.

I am indebted to all my student colleagues for their professional advice, in particular Ya Deng, Wei Wang, Jiudong Wu, Kuangda Wang, Yangping Zhao, Zoé-Lise Deck-Léger, Sulav Adhikari, and Nasser Ghassemi. It is a great pleasure to study and work with them.

I appriciate all the advice and help from my friends. They gave me the feeling of being at home when I was staying in Montrel.

I would like to thank all the jury members for their time and efforts in reviewing my thesis and providing me valuable comments.

Last but not least, I would like to thank my parents, who gave me the birth and brought me up. They always support me, listen to me and love me. I would like to express my deepest gratitude to the special and beautiful girl Katherine Li, for her endless love, encouragement and support.

RÉSUMÉ

Les taux de transmission des systèmes de communication sans-fil modernes augmentent. De nouvelles bandes de fréquences et de nouvelles technologies sont exploitées pour supporter de hauts taux de transmission. La bande d'ondes millimétriques est une bonne candidate pour supporter des taux de transmission de l'ordre des Gbps. De plus, la technologie à entrées/sorties multiples (MIMO) ouvre la porte à des systèmes de communication à bas coût à haut taux de transmission.

Le récepteur hétérodyne standard est utilisé dans plusieurs systèmes de communication, puisqu'il présente une grande sélectivité et une grande sensibilité. Par contre, le récepteur à conversion directe permet un meilleur niveau d'intégration en diminuant le nombre de composants des circuits. Parmi les récepteurs à conversion directe, ceux à six ports ont un circuit passif qui sert d'interferomètre. La diversité additionnelle est produite par les sorties en quadrature, qui sont des combinaisons linéaires du signal d'entrée et du signal de référence. Les guides d'onde intégrés au substrat (SIW) peuvent être facilement intégrés à des circuits planaires. La conception est simplifiée puisqu'il existe des méthodes de conception de guides d'ondes traditionnels. Un système MIMO à six ports de type SIW est présenté dans cette dissertation.

Premièrement, un diviseur de puissance et un coupleur hybride de type SIW sont présentés. L'implémentation de ces circuits, basée sur les règles de conception des structures SIW, est réalisée une bande de fréquence d'intérêt. Plusieurs paramètres critiques peuvent être manipulés pour contrôler les performances du diviseur de puissance et du coupleur hybride. Une transition de la structure SIW à la ligne micro-ruban est conçue pour permettre des mesures. Les résultats de simulation du circuit démontrent que celui-ci offre une bonne performance.

Deuxièmement, à partir du diviseur de puissance et du coupleur hybride, le circuit à six ports est présenté. Trois types d'architechtures sont comparées, et l'une d'elles est choisie pour le système de démonstration. Les résultats de simulation et les résultats expérimentaux concordent, et guarantissent une bonne performance du circuit proposé et du système de communication sans-fil dans lequel le circuit est intégré.

Finalement, le système de 2×2 ports est présenté. Il n'y a pas de couplage réciproque entre les deux récepteurs lorsque le critère de propagation de Rayleigh dans la ligne de visée est respecté.

Les multiples ports de sortie en quadrature du circuit à six ports garantissent que la performance du système MIMO sera acceptable lorsque des paramètres sont modifiés. Ceci peut être prouvé par le taux d'erreurs sur les bits dans différents cas.

ABSTRACT

Presently, the data rates in modern wireless communication systems are becoming higher and higher and new frequency bands and technologies are being exploited in support of high data transmissions. The millimeter-wave band is a candidate of choice to support Gbps data transmission. In addition, Multiple-Input Multiple-Output (MIMO) technology will open the way for low-cost reliable communication systems that require even higher data rates.

While the conventional heterodyne receiver has been widely applied in many kinds of communication systems due to its high selectivity and sensitivity, the direct-conversion receiver allows higher-level circuit integration by reducing the number of circuit components. Among these direct-conversion receivers, six-port scheme presents a passive circuit that acts as an interferometer. The additional diversity is produced by the quadrature outputs of the six-port circuit that are linear combinations of the unknown input signal and the reference signal. Substrate integrated waveguide (SIW) can be integrated with planar circuits easily. The design procedure is obviously simplified as a result of the existing typical design methods for the rectangular waveguide. Based on the above techniques and discussions, the millimeter-wave MIMO system based on SIW six-port circuit is presented in this dissertation.

First, the SIW power divider and hybrid coupler are presented. The implementation of those circuits is based on the SIW design rules, according to the working frequency band of interest. Several critical parameters can be manipulated to control performances of the SIW power divider and hybrid coupler. An SIW to microstrip line transition is designed for measurement purposes. Simulation results of the circuits show good performances.

Second, based on the studied and designed SIW power divider and hybrid coupler, the six-port circuit is presented. Three types of six-port architecture are compared, with one of them chosen to work in our millimeter-wave MIMO system demonstration. Simulation and measurement results agree well and guarantee a good performance of the proposed circuit itself and wireless high-speed communication system in which the circuit is embedded.

Finally, the 2×2 millimeter-wave MIMO system is presented. There will be no crosstalk between two receiver array responses when the line-of-sight (LoS) propagation Rayleigh criterion is satisfied. Multiple quadrature outputs of the six-port circuits ensure that the performance of the

MIMO system will stay acceptable when some parameters are changed. This can be proven by the bit error rates (BER) in different cases.

TABLE OF CONTENTS

LIST OF TABLES

LIST OF FIGURES

LIST OF ACRONYMS AND ABBREVIATIONS

ADS	Advanced design system
BBA	Baseband amplifier
BBM	Baseband module
BER	Bit error rate
BI-RME	Boundary integral-resonant mode expansion
BPSK	Binary phase shift keying
CMOS	Complementary metal oxide semiconductor
CPW	Coplanar waveguide
CW	Continuous wave
FCC	Federal communication commission
FMCW	Frequency modulation continuous wave
Gbps	Giga bit per second
HDMI	High definition multimedia interface
HFSS	High frequency structure simulator
IF	Intermediate frequency
LNA	Low noise amplifier
LO	Local oscillator
LoS	Line of sight
LPF	Low pass filter
Mbps	Mega bit per second
MHMIC	Miniaturized hybrid microwave integrated circuit
MIMO	Multiple-Input Multiple-Output
MMIC	Monolithic microwave integrated circuit

OAM	Orbital angular momentum
OFDM	Orthogonal frequency division multiplexing
PCB	Printed circuit board
PHEMT	Pseudoorphic high electron mobility transistor
QAM	quadrature amplitude modulation
QFN	Quad flat no-lead
QPSK	Quadrature phase shift keying
RF	Radio frequency
SDR	software defined radio
SHC	sample and hold circuit
SISO	Single-Input Single-Output
SIW	substrate integrated waveguide
SOI	silicon on insulator
SPM	six-port module

INTRODUCTION

With the increasing data rate in modern wireless communication system and the development of cellular and wireless local area networks at lower frequencies (1-5 GHz) that are struggling with the scarcity of spectrum, the millimeter-wave bands, having an ultra-wideband (UWB) spectrum at low cost, are an alternative to support Gbps-level data transmission in both indoor and outdoor environments. Furthermore, compared to microwave bands, the millimeter-wave counterparts have a critical advantage that wavelength and ratio between the bandwidth and the center frequency are reduced, in the case of comparable bandwidths and data rates. This leads to the miniaturization of UWB transceivers. In addition, the re-use of the millimeter-wave spectrum can be realized for secure wireless communication as a result of the strong free space signal attenuation over 60 GHz band, for example.

The Federal Communication Commission (FCC) introduced a number of years ago, an opening of 7 GHz unlicensed spectrum (57 – 64 GHz) in the V-band [1], in order to provide more options for short-range but high-data rate communications. This band could support multi-Gbps wireless communication systems over distances up to a mile, which could be high-speed home or office wireless network and entertainment, such as extremely fast downloading of files and movies via wireless Ethernet and wireless High Definition Multimedia Interface (HDMI).

Furthermore, in order to support longer distance wireless communications for semi-unlicensed point-to-point links, the FCC has already opened 13 GHz spectrum (71 – 76 GHz, 81 – 86 GHz, 92 – 95 GHz) in the E-band and W-band [2], avoiding the high oxygen absorption in the 60 GHz band (around 20 dB/Km, at the sea level). As a result, point-to point wireless local area network and broadband high speed Internet access are available, and rapid communication system recovery after disasters or interruptions can also be taken into account.

There have been a lot of previous works focusing on millimeter-wave wireless communications. Besides the high speed data rate, the successful integration of circuits and modules into the same substrate is also important, in order to reduce the cost and enhance the integration [3]. For example, Gallium Arsenide (GaAs) technology has been made use of in applications up to 110 GHz [4], [5]; Complementary Metal Oxide Semiconductor (CMOS) is another common and ideal solution in terms of cost and circuit integration for large-scale

production [6]; Silicon Germanium (SiGe), Bipolar CMOS (BiCMOS) can also provide good performances and keep low cost [6].

As the data rate in wireless communication system goes higher, we cannot rely on single millimeter-wave link any more. In this case, the use of a millimeter-wave Multiple-Input Multiple-Output (MIMO) technique will open the way for low-cost reliable multi-Gbps millimeter-wave communication systems [7]-[11], as shown in Figure 1. The sub-array is the basic module of a millimeter-wave MIMO system and should be able to achieve the required directivity toward the target receiver. In a line-of-sight (LoS) environment, when d (the distance between adjacent transmitters) and R (the distance between the transmitter and the receiver) are set up to satisfy Rayleigh criterion [12], there is no crosstalk between any two receiver array responses.

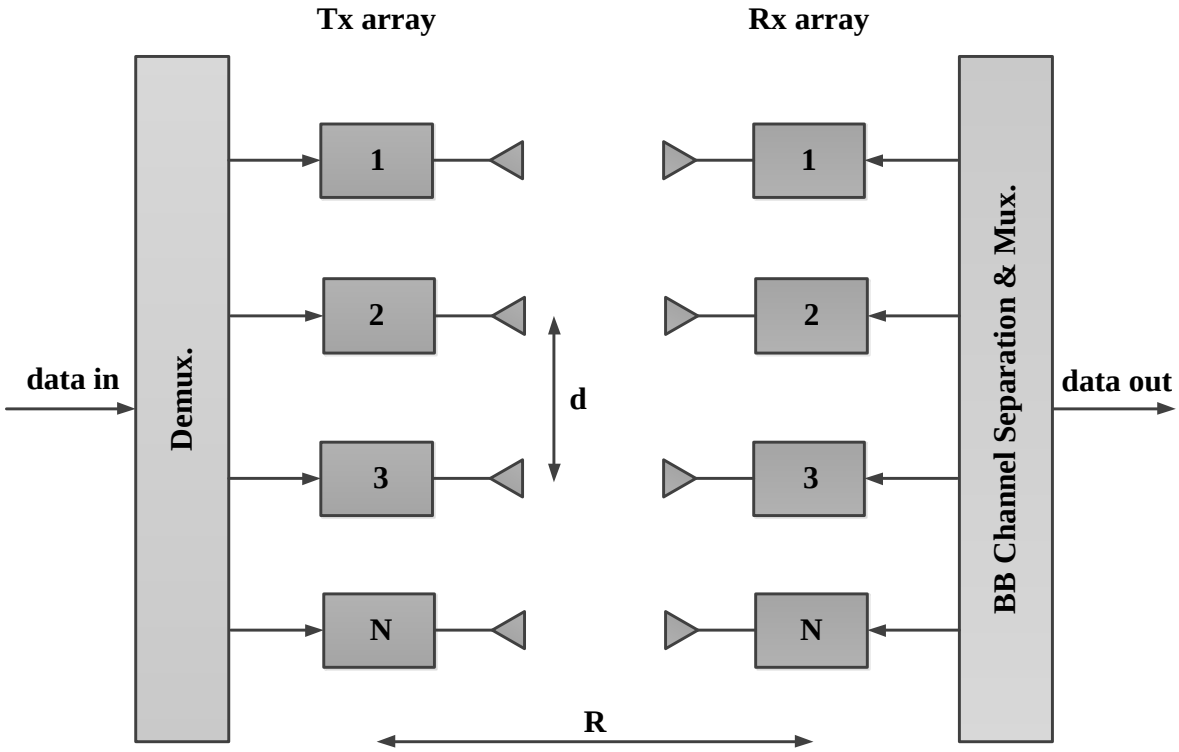

Figure 1 MIMO system architecture

Millimeter-wave MIMO systems differ from their counterparts at lower frequency bands [13], [14]. The channels are LoS or near LoS in this case. Therefore, spatial multiplexing can no longer be obtained through the multipath effect which is available in a rich scattering environment. Instead, the appropriate method for millimeter-wave MIMO spatial multiplexing is to focus the receiver on the different transmitter antenna to obtain independent parallel channels [15]-[17].

Six-port [18], [19] is a passive circuit that works as an interferometer. The four output signals are linear combinations of the unknown input signal and the reference signal. Six-port can realize quadrature down-conversion (including direct down-conversion and heterodyne down-conversion) or direct modulation by using appropriate devices. Several significant advantages come from its intrinsic properties and determine that it is the right candidate of the proposed millimeter-wave MIMO system:

- Wide bandwidth
- Reduced local oscillator power requirement
- Very good isolation between radio frequency (RF) inputs

It will be proved that the six-port interferometry adds supplementary quadrature diversity to the system. The inherent MIMO spatial and additional quadrature diversity (due to six-port interferometry) allows a possibility to choose the best BER (bit error rate) value out of the four output combinations when the distance changes versus the optimal Rayleigh value.

The substrate integrated waveguide (SIW) structure [20] is a typical rectangular waveguide in planar form that is filled with dielectric material by two arrays of metallic holes. It is very useful in the system applications that require low cost, low insertion loss, high power capability and easy integration structure. Usually, the integration with planar circuits is quite common and easy to make, such as coplanar waveguide (CPW) and microstrip line. Therefore, the SIW structure is appropriate for the design of the six-port circuit by applying the rectangular waveguide design process.

Based on the analysis of four technologies (millimeter-wave system, MIMO, six-port receiver, SIW structure), millimeter-wave MIMO systems based on SIW six-port technology are proposed. At first, the millimeter-wave SIW components are analyzed and designed in detail. Then, the entire millimeter-wave SIW six-port circuit is presented, based on the previous analysis and design of the power divider and hybrid coupler. In the end, the 2×2 millimeter-wave MIMO system based on SIW six-port receivers is presented and system simulation results are discussed. The system shows an improved demodulation results in various cases.

The thesis is organized in the following way:

In chapter 1, the studies of the SIW structure are reviewed and discussed. Some properties of the SIW structure, including low cost, easy integration with planar circuits, are considered critical to determine its application in design and development of the wanted six-port circuit. In addition, by using the existing design methods for the rectangular waveguide filled by the same dielectric as the SIW substrate, the design procedure of SIW circuits can be simplified. In order to design an SIW six-port circuit, the SIW power divider and the SIW hybrid coupler are studied in the beginning as building blocks. Various parameters of these two components are examined in order to optimize their performances. Once they are applied in the development of an entire six-port case, the required dimension can be found immediately, which saves a lot of design time and improves the design efficiency. In order to measure the six-port circuit, an SIW to microstrip line transition is designed.

In chapter 2, the six-port circuit is reviewed and discussed. The advantages of the six-port circuit make it an outstanding candidate for the proposed millimeter-wave MIMO communication system. Three types of six-port junction are analyzed. Following a parametrical study, the final six-port circuit is presented, based on the previous analysis of the SIW power divider and hybrid coupler. The simulation and measurement results agree well, and show that the proposed six-port circuit can work at the required frequency band, making it possible to be applied in the MIMO system.

In chapter 3, a basic millimeter-wave 2×2 MIMO system is presented and discussed. The millimeter-wave MIMO wireless communication system possesses the advantage of high speed transmission that differs from the MIMO systems at lower frequency bands. The multiple

quadrature outputs of the two six-port receivers provide the possibility that the performance of the proposed millimeter-wave MIMO system could be improved even if some distances between transmitters and receivers are not in agreement with the Rayleigh criterion. This provides an additional degree of freedom for the proposed MIMO system. The system shows a good BER performance.

The contributions of the work presented in this thesis are summarized in the last chapter. Although only the millimeter-wave 2×2 MIMO system is presented in this work, it is possible that the analysis and design method can be used in other types of MIMO systems.

CHAPTER 1 ANALYSIS AND DESIGN OF MILLIMETER-WAVE SUBSTRATE INTEGRATED WAVEGUIDE CIRCUIT COMPONENTS

1.1 Introduction

Rectangular waveguide components have been used in millimeter wave circuits and systems. Especially, they can be used to design high-Q components. However, their relatively high cost and difficult integration with other circuit components have prevented themselves from being widely used in low-cost mass-producible systems. Different kinds of complex transitions [21]-[24] have been reported to satisfy the demand for integration with planar circuits, such as microstrip line and coplanar waveguide (CPW). However, typical integration schemes between rectangular waveguide and planar circuits are bulky and usually need precise machining process, which is especially difficult at millimeter wave frequencies.

Substrate integrated waveguide (SIW) structure has been proposed and studied recently as an alternative technology in low cost, low insertion loss, high power capability and easy integration applications. This is an appropriate technology to design microwave and millimeter wave components and sub-systems although the Q factor of the waveguide is slightly reduced because of the dielectric filling, reduced height and influence of metallic holes. The entire circuits, including other planar circuits, transitions and SIW structures can then be fabricated on the same substrate by using standard printed circuit board (PCB) technology or other planar fabrication technologies.

The SIW structure is a type of rectangular waveguide filled with dielectric material bounded by two arrays of metallic holes. The periodic metallic holes bring up difficulty in analyzing the performance of the waveguide, compared to simple metal walls of the conventional rectangular waveguide. However, the analysis procedure can be made much more convenient if the SIW structure is transformed to an equivalent rectangular waveguide filled with the same dielectric material with a special ratio of width/height according to the size of the targeted SIW structure. What is more, the propagation characteristics of SIW can be obtained by applying a generalized boundary integral-resonant mode expansion (BI-RME) method [25]. It was demonstrated that a TE_{10}-like mode of the SIW structure has the same dispersion characteristics as the TE_{10} mode of

the rectangular waveguide filled with the same dielectric material with an equivalent width. The equivalent width can be calculated as follows:

$$a_{eqv} = a - \frac{d^2}{0.95 \cdot b} \tag{1.1}$$

The geometry of the SIW structure is described in Figure 1.1, where *h* is the thickness of dielectric substrate, *d* is the diameter of metallic holes, *b* is the distance between two adjacent holes, *a* is the physical width of SIW, and a_{eqv} is the equivalent width of SIW. For a SIW structure, *h* could be less than half of the width, and it remains the same when the SIW structure is transformed to an equivalent rectangular waveguide.

Based on these properties of the SIW structure, existing design methods for the rectangular waveguide can be made use of to analyze and design the SIW components if the equivalent width a_{eqv} has been already known and can be re-used here.

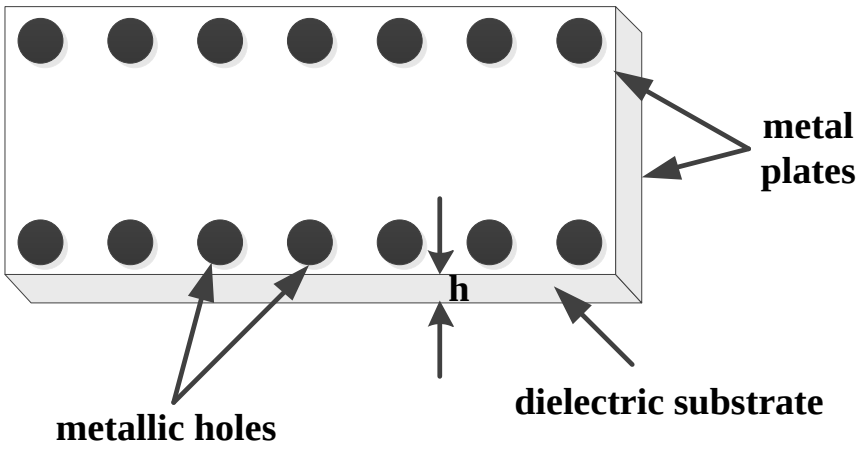

(a)

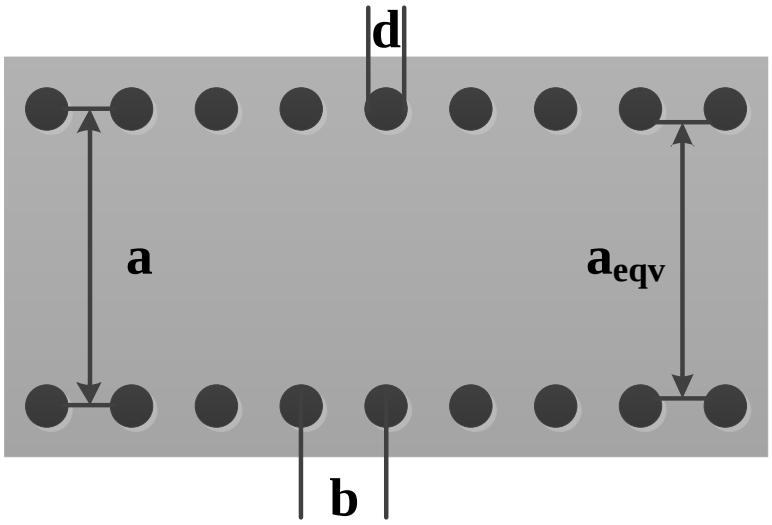

(b)

Figure 1.1 Topology of the SIW structure (a) solid view; (b) top view

A number of millimeter wave SIW components are presented in this chapter. They are analyzed and designed based on the equivalent rectangular waveguide, as discussed before. By using commercial software high frequency structure simulator (HFSS) 15.0 of ANSOFT, these components are designed and optimized over the 55-65 GHz frequency range. A Rogers RT/duroid 6002 Laminates substrate is used in the simulation with dielectric permittivity of 2.94 and substrate thickness of 10 mils.

1.2 SIW power divider

The geometry of the SIW H-plane power divider is shown in Figure 1.2. A straight Y-junction [26] is adopted in the proposed power divider. The Y-junction consists of a bifurcated waveguide fed by a symmetrical step junction. Assuming that the dimension of SIW is chosen to support the TE_{10} mode exclusively in the selected frequency range, the total reflection of the TE_{20} mode will occur, because there will be no TE_{10} mode on either side of the symmetrical step junction excited by the TE_{20} mode due to the asymmetry of the TE_{20} mode on the discontinuity part.

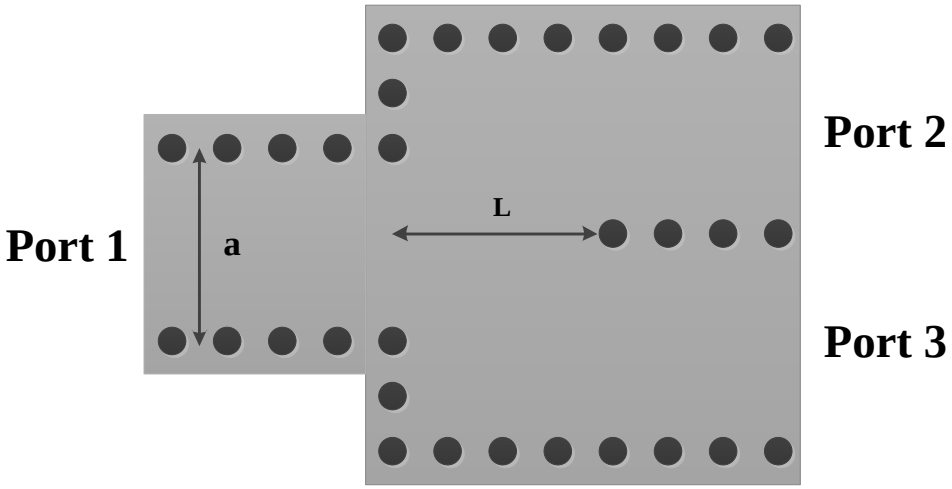

Figure 1.2 Geometry of the SIW power divider

The width of the input and output SIW can be calculated according to the dielectric permittivity of the substrate and the center frequency of the power divider:

$$a_{eqv} = \frac{c}{2f_c\sqrt{\varepsilon_r}} \tag{1.2}$$

Where f_c is the cutoff frequency of the SIW structure, ε_r is the relative dielectric constant of the substrate.

Distance L between the two discontinuities can be optimized to achieve the following goals:

- Minimize the reflection coefficient S_{11} at port 1
- Keep the magnitudes of transmission coefficients S_{21} and S_{31} equal and close to -3 dB
- Keep S_{21} and S_{31} in phase over the frequency range

To evaluate the performance of the proposed power divider, S parameter simulation is executed by means of software HFSS. The center frequency is chosen at 60 GHz. Parameters of the power divider are listed in Table 1.1. The simulated S parameter results are shown in Figure 1.3 ~ Figure 1.5.

Figure 1.3 shows that the magnitude of S_{11} is better than 20 dB over the 55-65 GHz frequency range. Figure 1.4 shows that the transmission coefficients at different output ports are both around 3.3 dB, proving that the power split ratio is 1:1. Figure 1.5 shows that the signals at these two ports are in phase (the two curves are superposed).

Table 1.1 Dimension of the SIW power divider

Parameter	Value
ε_r	2.94
b	0.508 mm
d	0.254 mm
h	0.254 mm
a_{eqv}	2.6 mm
a	2.73 mm
L	3.7 mm

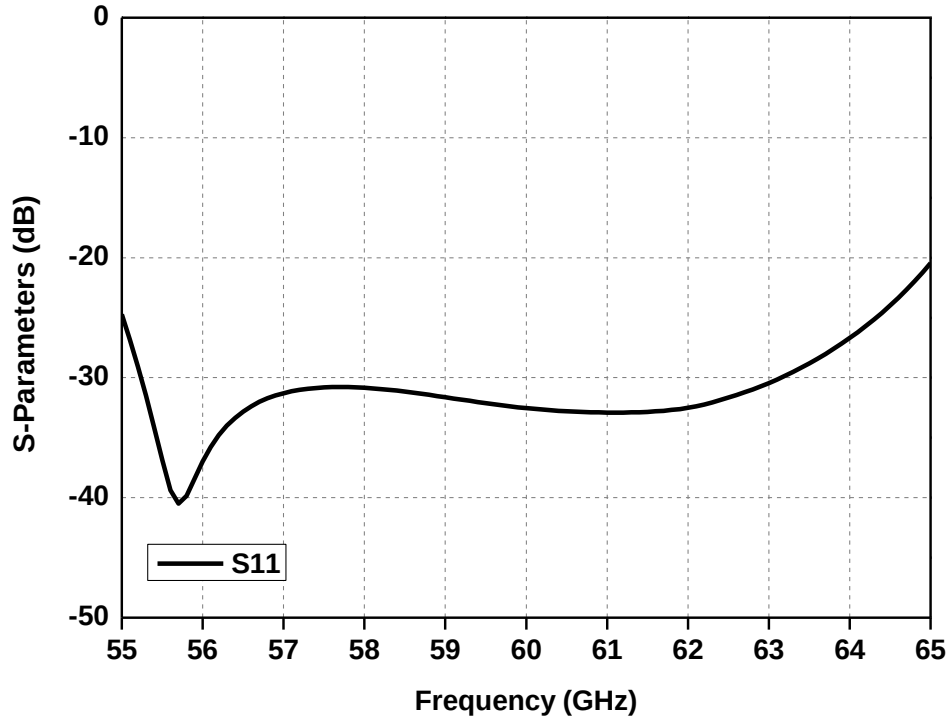

Figure 1.3 Simulated magnitude of S_{11} of the SIW power divider

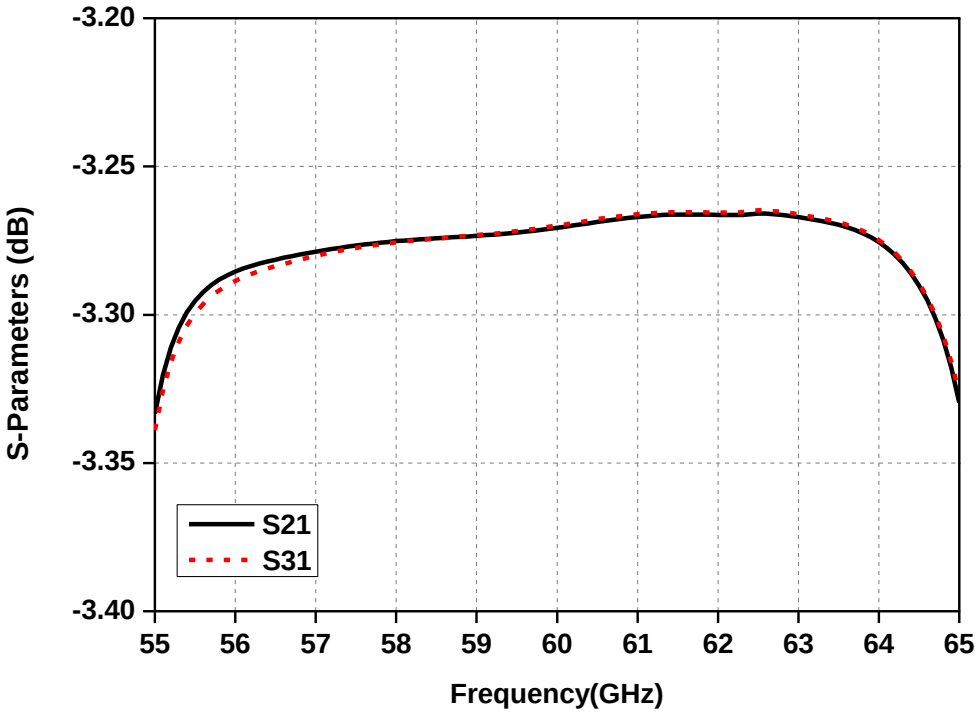

Figure 1.4 Simulated magnitudes of transmission coefficients of the power divider

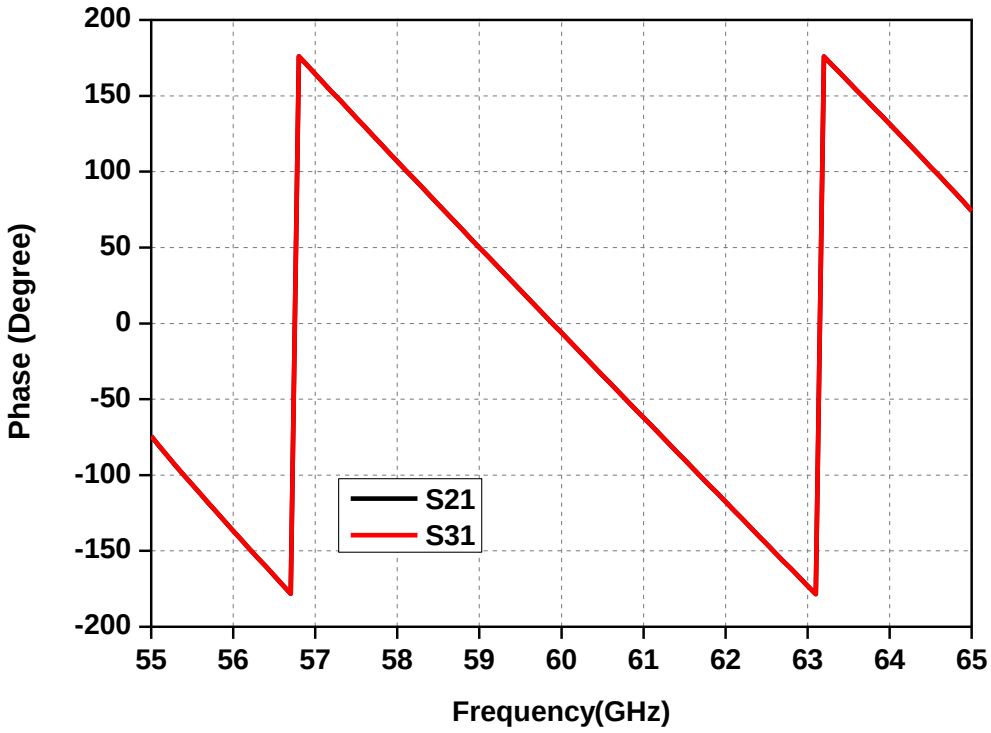

Figure 1.5 Simulated phases of transmission coefficients of the power divider

The electric field distribution is shown in Figure 1.6. It can be seen that the magnitudes of electric field at two output ports are the same. Furthermore, they are in phase.

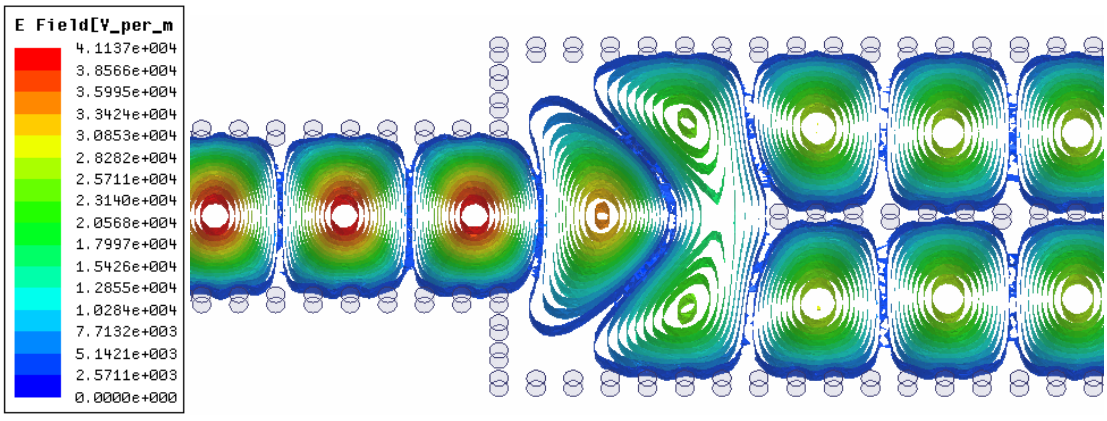

Figure 1.6 Electric field distribution of the power divider

1.3 SIW hybrid coupler

The geometry of the targeted SIW hybrid coupler is shown in Figure 1.7. It is composed of two SIWs with a common wall on which an aperture is utilized to realize the coupling between the two SIWs at the output ports. The metallic vias close to the aperture are moved towards the aperture to control the coupling coefficient.

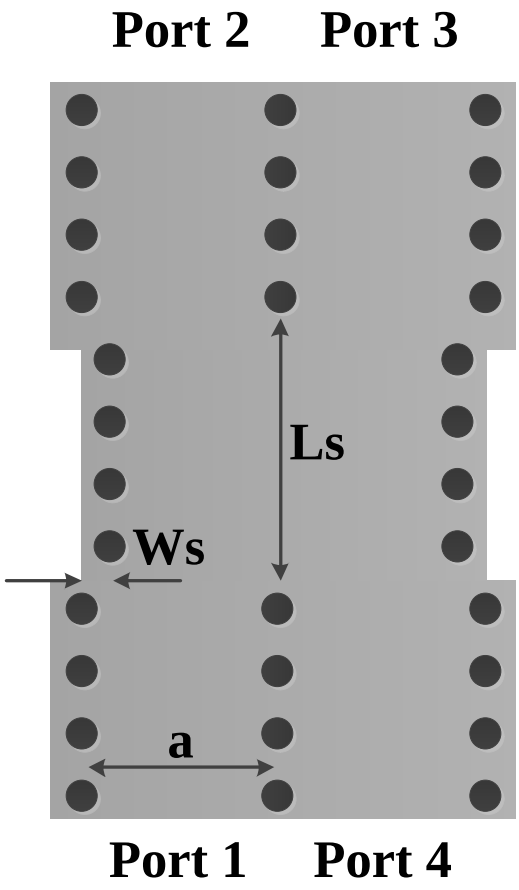

Figure 1.7 Geometry of the SIW hybrid coupler

The width of the SIW hybrid coupler is the same as that of the SIW power divider. Step width *Ws* and aperture length *Ls* are optimized to achieve the following coupling, reflection and isolation requirements:

- Minimize the reflection coefficient S_{11} at the port 1 and the isolation coefficient S_{41} between the port 1and the port 4
- Keep the magnitudes of the transmission coefficients S_{21} and S_{31} equal and close to -3 dB
- Keep the difference between the phases of S21 and S31 90° over the frequency range

S-parameters simulation of the designed coupler is made in HFSS at the center frequency 60 GHz. Parameters of the hybrid coupler are listed in Table 2.2. The simulated S parameter results are shown in Figure 1.8 ~ Figure 1.10.

Table 1.2 Dimensions of the SIW hybrid coupler

Parameter	Value
ε_r	2.94
b	0.508 mm
d	0.254 mm
h	0.254 mm
a_{eqv}	2.6 mm
a	2.73 mm
Ls	2.7 mm
Ws	0.78 mm

Figure 1.8 shows that the magnitude of S_{11} is better than 20 dB at 60 GHz and better than 17 dB over the frequency range, while the isolation between port 1 and port 4 is also better than 20 dB over the frequency range. Figure 1.9 shows that the transmission coefficients at port 2 and port 3 are both 3.3 dB, validating that the coupling ratio is 1:1. The difference between the phases of these two ports is close to 90° (89.7° at 60.5GHz), which agrees with the theoretical value very well.

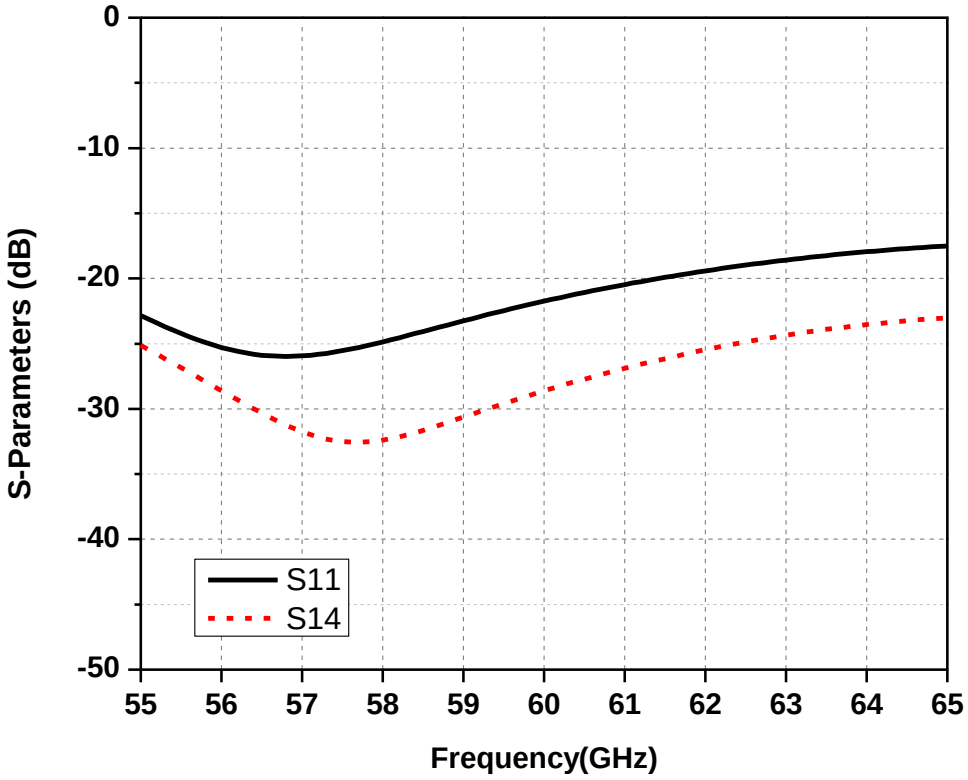

Figure 1.8 Simulated magnitudes of S_{11} and isolation between port 1 and port 4

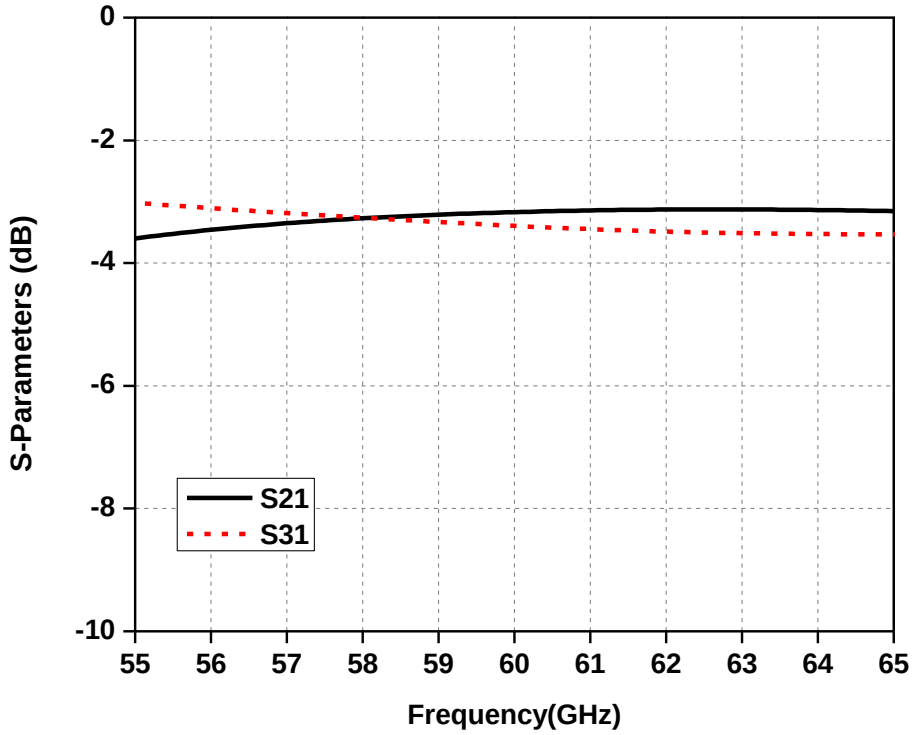

Figure 1.9 Simulated magnitudes of transmission coefficients of the hybrid coupler

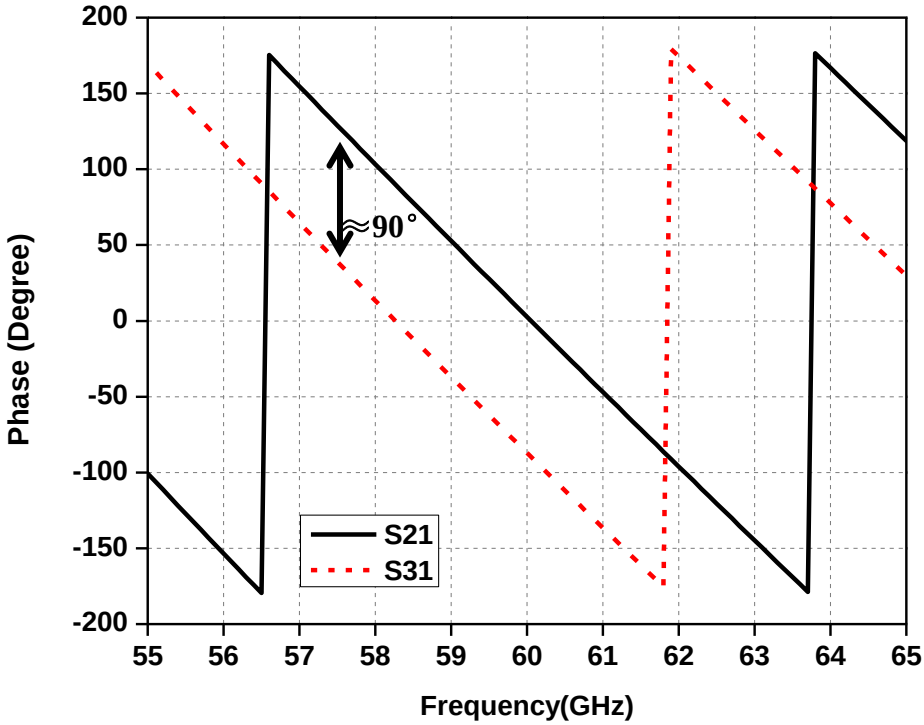

Figure 1.10 Simulated phases of transmission coefficients of the hybrid couple

The electric field distribution is shown in Figure 1.11. It can be seen that the magnitudes of electric field at port 2 and port 3 are the same. Furthermore, there is a time delay in the output of port 3.

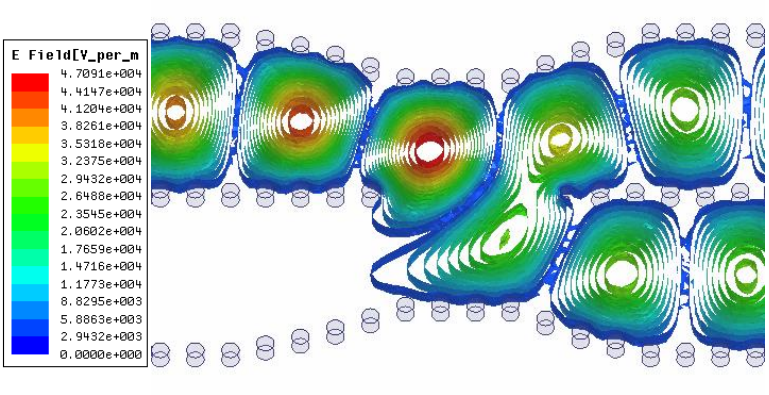

Figure 1.11 Electric field distribution of the hybrid coupler

1.4 SIW to microstrip line transition

Transitions from SIW to microstrip line are used to make the impedance matching at each port of the six-port circuit [27]. The tapered microstrip line transforms the TE mode in the SIW section to the quasi-TEM mode of the microstrip line. The geometry of a back-to-back SIW to microstrip line transition is shown in Figure 1.12.

Figure 1.12 Geometry of the transition

Length *Lm* and width *Wm* of the tapered part can be optimized to achieve the following goals:

- Minimize the reflection coefficient S_{11} at the port 1
- Minimize the insertion loss S_{21} of the transition

To evaluate the performance of the transition, a back-to-back structure is designed and its S-parameters simulation is made in HFSS at the center frequency 60 GHz. The parameters of the power divider are listed in Table 1.3. The simulated S parameter results are shown in Figure 1.13 ~ Figure 1.14.

Table 1.3 Dimensions of the transition

Parameter	Value
ε_r	2.94
b	0.508 mm
d	0.254 mm
h	0.254 mm
W	0.66 mm
Wm	1.02 mm
Lm	0.98 mm

Figure 1.13 shows that the magnitude of S_{11} is better than 35 dB over the 55-65 GHz frequency range. Figure 1.14 shows that the insertion loss between the input port and the output port of the transition is better than 0.3 dB over the frequency range. These results suggest that the transition has little influence on the whole six-port circuit.

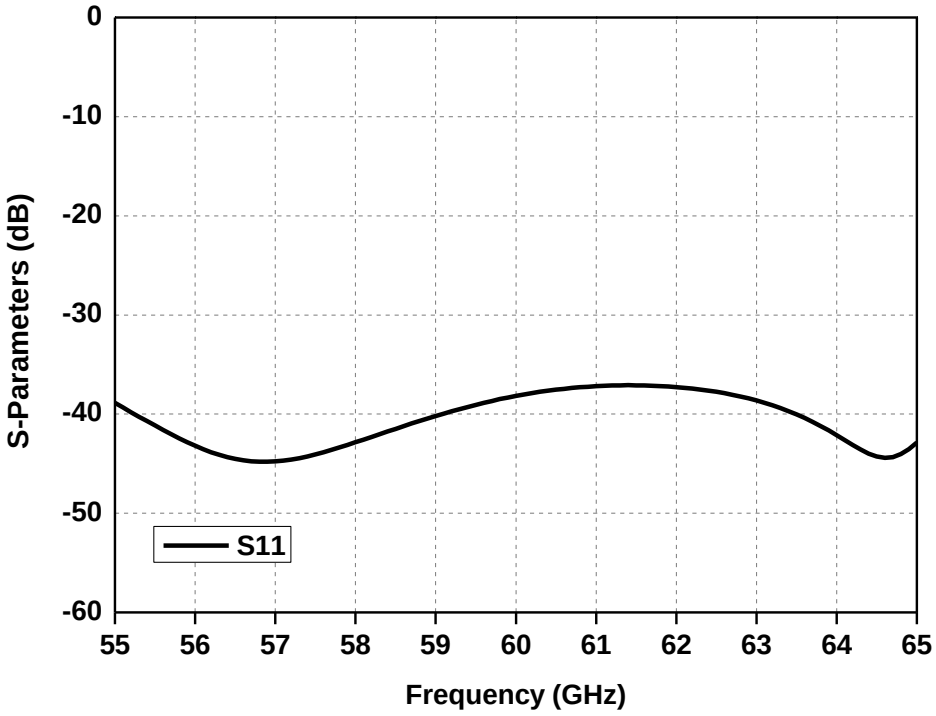

Figure 1.13 Simulated magnitude of $S_{11}$of the transition

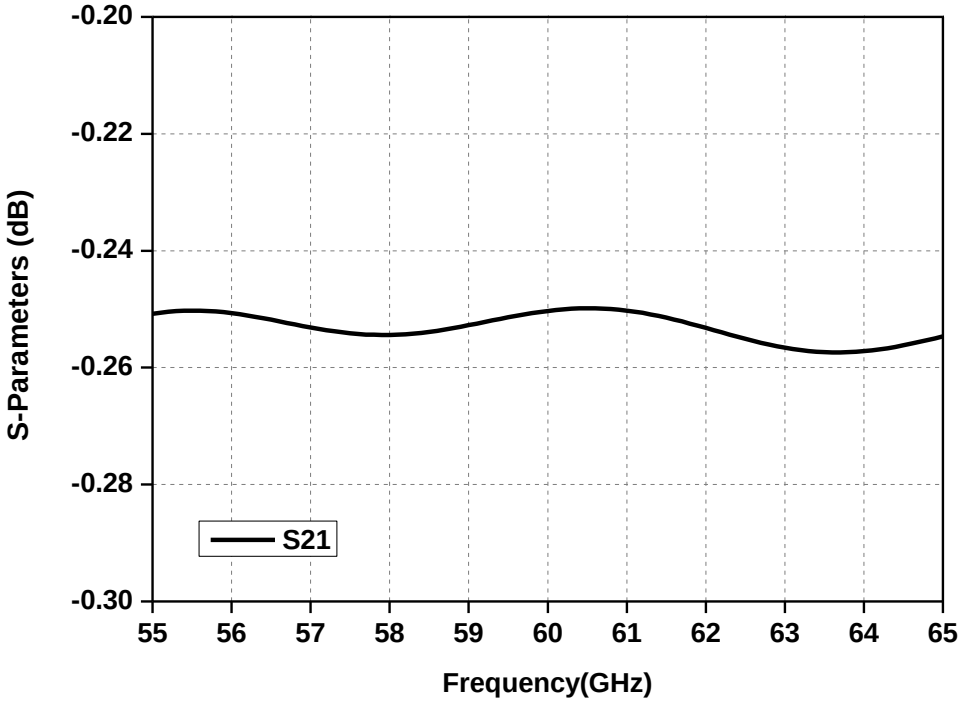

Figure 1.14 Simulated insertion loss of the SIW power divider

The electric field distribution is shown in Figure 1.15. It can be seen that the electromagnetic field goes through the transition smoothly without a large reflection loss or a large insertion loss.

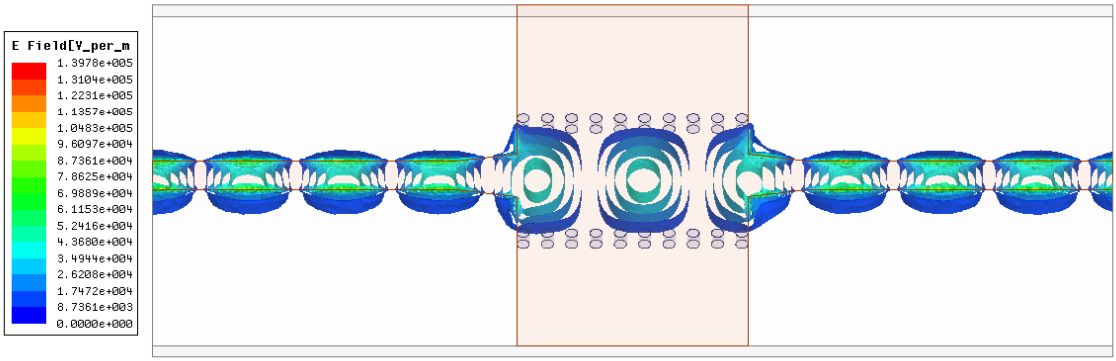

Figure 1.15 Electric field distribution of the transition

CHAPTER 2 MILLIMETER-WAVE SUBSTRATE INTEGRATED WAVEGUIDE SIX-PORT CIRCUIT DESIGN

2.1 Introduction

The six-port circuits have been studied and developed since the 1970s [28]-[32]. It was first used by Cohn and Weinhouse to measure the phase of a microwave signal, and then developed by Engen and Hoer to obtain the complex reflection coefficients of a signal in microwave analysis. The six-port technologies were further developed by Professor R. G. Bosisio and collaborators, used as a microwave and millimeter-wave demodulator [33]. The six-port is a passive circuit, composed of hybrid couplers and/or power dividers with or without phase shifters. It has two inputs, one for the unknown signal and the other for the reference signal, and four outputs of linear combinations of two input signals.

Until now, six-port circuits have been developed in many applications. It can be utilized as both standard frequency modulation continuous wave (FMCW) radar sensor and direct down-conversion receiver. In addition, the six-port receiver can demodulate signals in different formats, including binary phase shift keying (BPSK), quadrature phase shift keying (QPSK), and quadrature amplitude modulation (QAM). Previous studies show that six-port circuits can be implemented with different fabrication technologies. For example, miniaturized hybrid microwave integrated circuit (MHMIC) and monolithic microwave integrated circuit (MMIC) technology were used for QPSK demodulation in Ka-band six-port front end modules [34], machined WR-10 waveguides were used for the design of a collision avoidance continuous wave (CW) radar sensor in W-band [35], SIW structure was also used for QPSK, QAM16 and orthogonal frequency division multiplexing (OFDM) demodulation in Ka-band software defined radio (SDR) receivers [36]-[37], and so on.

Millimeter-wave six-port circuit is an innovative approach in wireless communication. Many previous research results demonstrated that the six-port down-converter can work well when the local oscillator (LO) power is as low as -25 dBm, compared to conventional techniques with anti-parallel diodes (the LO power is at least +10 dBm for achieving the same conversion loss). The excellent isolation between the unknown signal and the reference signal (up to 40 dB in certain implementations) is another important advantage.

The entire six-port circuit is presented in this chapter. It is designed based on the previous analysis and design of the millimeter-wave SIW power divider and hybrid coupler. By using commercial software HFSS 15.0, the six-port circuit is designed and optimized over the 60-63 GHz frequency range.

2.2 Six-port circuit theory

In the previous studies, six-port circuits have been demonstrated as an excellent candidate for microwave and millimeter-wave modulator and demodulator for both communication and radar systems.

When the six-port circuits work as modulators, the outputs of the hybrid couples are connected to two pairs of mono-ports, having adjustable reflection coefficients. Different modulation signals (such as QPSK, 8PSK, and 16QAM) can be obtained by using different reflection coefficients that are only real part values. For example, the QPSK signal is produced if the pair of reflection coefficients is 1 and -1 (open and short circuits, respectively).

When they work as demodulators, there are three types of block diagrams to design and apply six-port circuits according to the design situation as follows:

- Three couplers + power divider
- Two couplers + two power dividers + 90 ° phase shifter
- Four couplers + 90 ° phase shifter

The three types of six-port circuit have been widely applied at microwave and millimeter-wave frequency. Each of them has its own features, including advantages and disadvantages:

- For the first type, no phase shifter is required.
- For the second type, no additional matching load is required.
- For the third type, no power divider is required.

The block diagrams of different types of six-port circuit are shown in Figure 2.1.

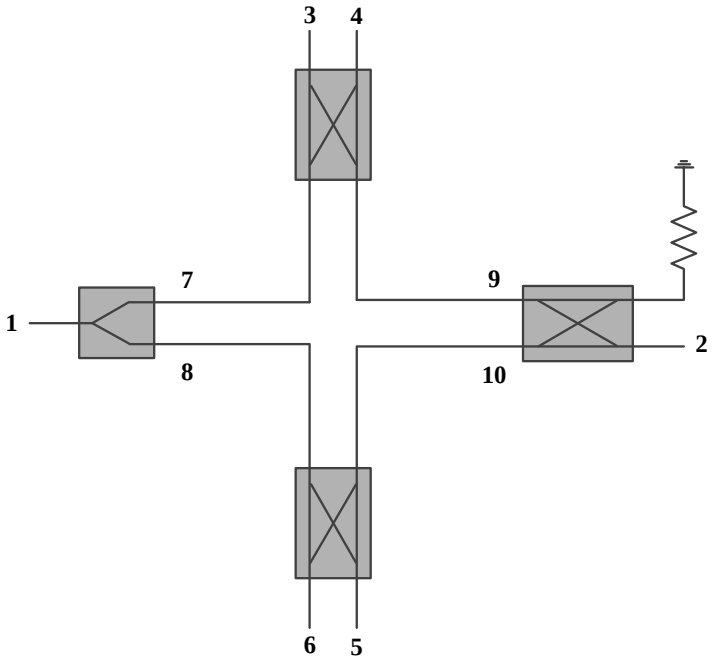

(a) Type 1

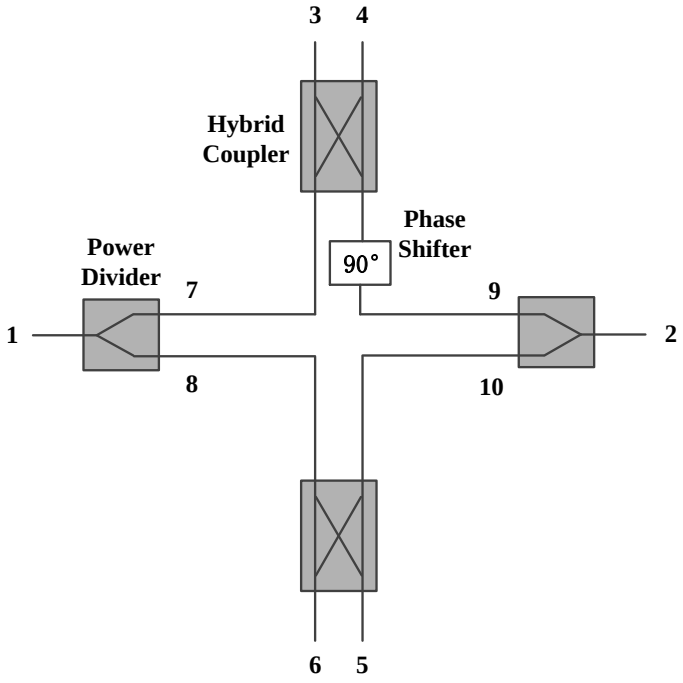

(b) Type 2

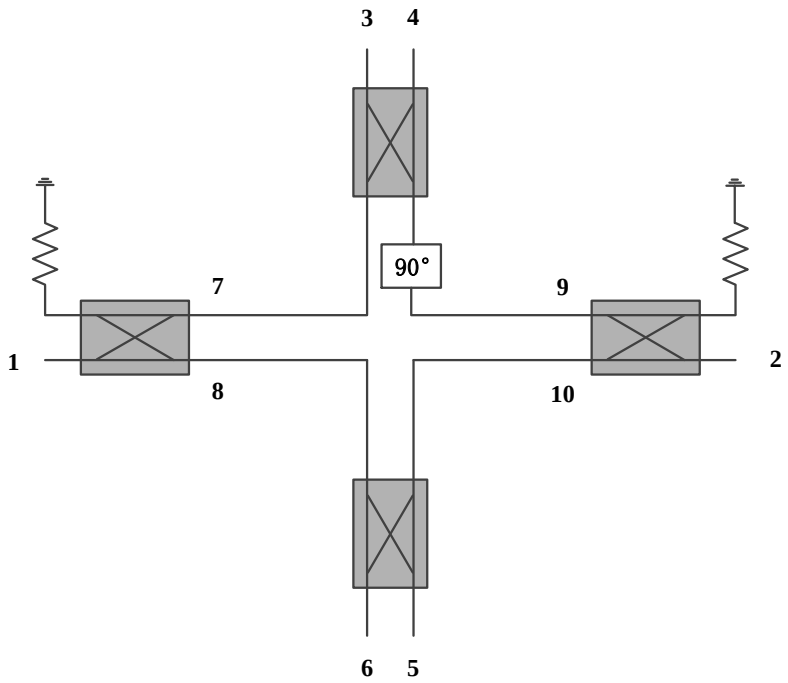

(c) Type 3

Figure 2.1 Block diagram of three types of six-port circuit

The analysis of the six-port circuit is shown by calculating the S parameter matrix of the first type. The other two types of six-port junctions can be analyzed through the same process.

The S parameter matrix of the power divider is given in 2.1:

$$S = -j\frac{1}{\sqrt{2}}\begin{bmatrix} 0 & 1 & 1 \\ 1 & 0 & 0 \\ 1 & 0 & 0 \end{bmatrix} \tag{2.1}$$

The S parameter matrix of the hybrid coupler is given in 2.2:

$$S = -\frac{1}{\sqrt{2}} \begin{bmatrix} 0 & j & 1 & 0 \\ j & 0 & 0 & 1 \\ 1 & 0 & 0 & j \\ 0 & 1 & j & 0 \end{bmatrix} \tag{2.2}$$

To obtain the S parameter matrix of the entire six-port junction, all the input ports, the intermediate ports and the output ports are numbered, as shown in Figure 2.1. The incident wave and reflected wave at each port are defined as a_n and b_n, $n = 1, 2, \cdots, 10$.

From 2.1 and 2.2, the incident waves at port 7 to port 10 can be expressed as:

$$b_7 = -j\frac{1}{\sqrt{2}}a_1$$

$$b_8 = -j\frac{1}{\sqrt{2}}a_1$$

$$b_9 = -\frac{1}{\sqrt{2}}a_2 \tag{2.3}$$

$$b_{10} = -j\frac{1}{\sqrt{2}}a_2$$

Then the reflected waves at port 1 to port 6 can be expressed as:

$$b_1 = 0$$

$$b_2 = 0$$

$$b_3 = \frac{1}{2}(-a_1 + a_2)$$

$$b_4 = \frac{1}{2}(ja_1 + ja_2) \tag{2.4}$$

$$b_5 = \frac{1}{2}(ja_1 - a_2)$$

$$b_6 = \frac{1}{2}(-a_1 + ja_2)$$

Since

$$[b] = [S][a] \tag{2.5}$$

The S parameter matrix of the first type can be listed as follows:

$$\begin{bmatrix} b_1 \\ b_2 \\ b_3 \\ b_4 \\ b_5 \\ b_6 \end{bmatrix} = \frac{1}{2} \begin{bmatrix} 0 & 0 & -1 & j & j & -1 \\ 0 & 0 & 1 & j & -1 & j \\ -1 & 1 & 0 & 0 & 0 & 0 \\ j & j & 0 & 0 & 0 & 0 \\ j & -1 & 0 & 0 & 0 & 0 \\ -1 & j & 0 & 0 & 0 & 0 \end{bmatrix} \begin{bmatrix} a_1 \\ a_2 \\ a_3 \\ a_4 \\ a_5 \\ a_6 \end{bmatrix} \tag{2.6}$$

The S parameters of the other types of six-port junction can be calculated in the same way as the first one:

For model 2, the incident waves at the intermediate ports can be expressed as:

$$b_7 = -j\frac{1}{\sqrt{2}}a_1$$

$$b_8 = -j\frac{1}{\sqrt{2}}a_1$$

$$b_9 = -j\frac{1}{\sqrt{2}}a_2 \tag{2.7}$$

$$b_{10} = -j\frac{1}{\sqrt{2}}a_2$$

The reflected waves at the output ports are expressed as:

$$b_1 = 0$$

$$b_2 = 0$$

$$b_3 = \frac{1}{2}(-a_1 + a_2)$$

$$b_4 = \frac{1}{2}(ja_1 + ja_2) \tag{2.8}$$

$$b_5 = \frac{1}{2}(ja_1 - a_2)$$

$$b_6 = \frac{1}{2}(-a_1 + ja_2)$$

The S parameter matrix of the second type can be listed as follows:

$$\begin{bmatrix} b_1 \\ b_2 \\ b_3 \\ b_4 \\ b_5 \\ b_6 \end{bmatrix} = \frac{1}{2}\begin{bmatrix} 0 & 0 & -1 & j & j & -1 \\ 0 & 0 & 1 & j & -1 & j \\ -1 & 1 & 0 & 0 & 0 & 0 \\ j & j & 0 & 0 & 0 & 0 \\ j & -1 & 0 & 0 & 0 & 0 \\ -1 & j & 0 & 0 & 0 & 0 \end{bmatrix}\begin{bmatrix} a_1 \\ a_2 \\ a_3 \\ a_4 \\ a_5 \\ a_6 \end{bmatrix} \tag{2.9}$$

For model 3, the incident waves at the intermediate ports can be expressed as:

$$b_7 = -\frac{1}{\sqrt{2}} a_1$$

$$b_8 = -j\frac{1}{\sqrt{2}} a_1$$

$$b_9 = -\tfrac{1}{\sqrt{2}} a_2 \qquad (2.10)$$

$$b_{10} = -j\tfrac{1}{\sqrt{2}} a_2$$

The reflected waves at the output ports are expressed as:

$$b_1 = 0$$

$$b_2 = 0$$

$$b_3 = \tfrac{1}{2}(ja_1 - ja_2)$$

$$b_4 = \tfrac{1}{2}(a_1 + a_2) \qquad (2.11)$$

$$b_5 = \tfrac{1}{2}(ja_1 - a_2)$$

$$b_6 = \tfrac{1}{2}(-a_1 + ja_2)$$

The S parameter matrix of the third type can be listed as follows:

$$\begin{bmatrix} b_1 \\ b_2 \\ b_3 \\ b_4 \\ b_5 \\ b_6 \end{bmatrix} = \frac{1}{2} \begin{bmatrix} 0 & 0 & j & 1 & j & -1 \\ 0 & 0 & -j & 1 & -1 & j \\ j & -j & 0 & 0 & 0 & 0 \\ 1 & 1 & 0 & 0 & 0 & 0 \\ j & -1 & 0 & 0 & 0 & 0 \\ -1 & j & 0 & 0 & 0 & 0 \end{bmatrix} \begin{bmatrix} a_1 \\ a_2 \\ a_3 \\ a_4 \\ a_5 \\ a_6 \end{bmatrix} \tag{2.12}$$

The phases from two input ports to four output ports are critical in order to determine the demodulation results of the six-port junction. The phases can be obtained from the S parameter matrix. For example, for the first type, the phase differences between adjacent output ports are shown as follows:

$$\begin{aligned} ang(S_{32}) - ang(S_{31}) &= 180° \\ ang(S_{42}) - ang(S_{41}) &= 0° \\ ang(S_{52}) - ang(S_{51}) &= 90° \\ ang(S_{62}) - ang(S_{61}) &= -90° \end{aligned} \tag{2.13}$$

The three previous S parameter matrices are generated for the ideal cases that all the input ports and output ports are connected to perfect matching loads. However, in the application of a six-port receiver, four output ports are connected to other circuits such as power detectors, which sometimes have a limited matching condition. In these cases, a matching network is necessary to reduce undesired reflections.

2.3 SIW six-port circuit

The topology of the proposed SIW six-port circuit is shown in Figure 2.2. It consists of two SIW power dividers [38], two SIW hybrid couplers and the $\pm 45°$ phase shifters. The $\pm 45^\circ$ phase shifters are realized by the additional SIW transmission lines. There are four circular corners after the power dividers to lead the signal to the hybrid couplers. SIW to microstrip line transitions are applied at each port of the six-port circuit for measurement purpose. The output ports of the hybrid coupler are bent and separated enough to support the use of V connectors (with a 0.375 inch square flange). The layout of the whole SIW six-port circuit is shown in Figure 2.3.

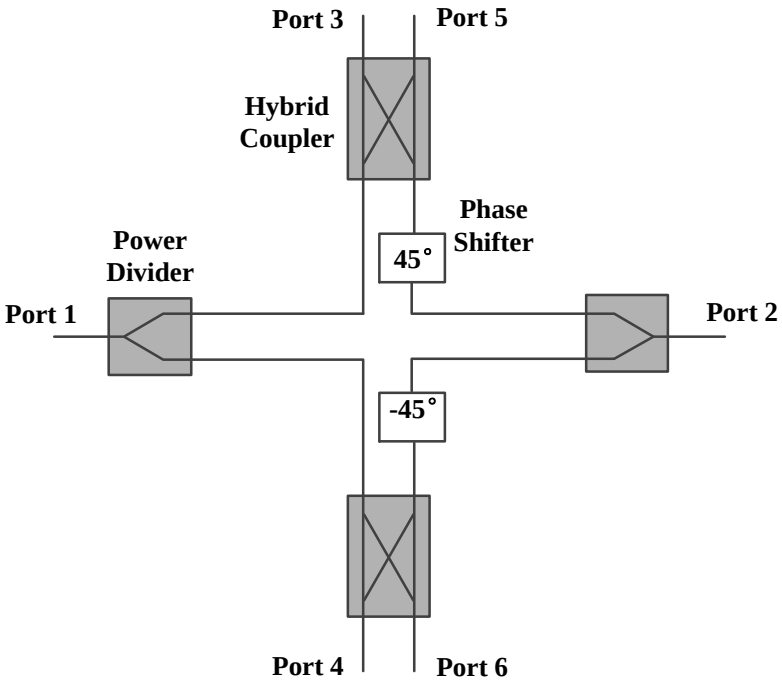

Figure 2.2 Topology of the SIW six-port circuit

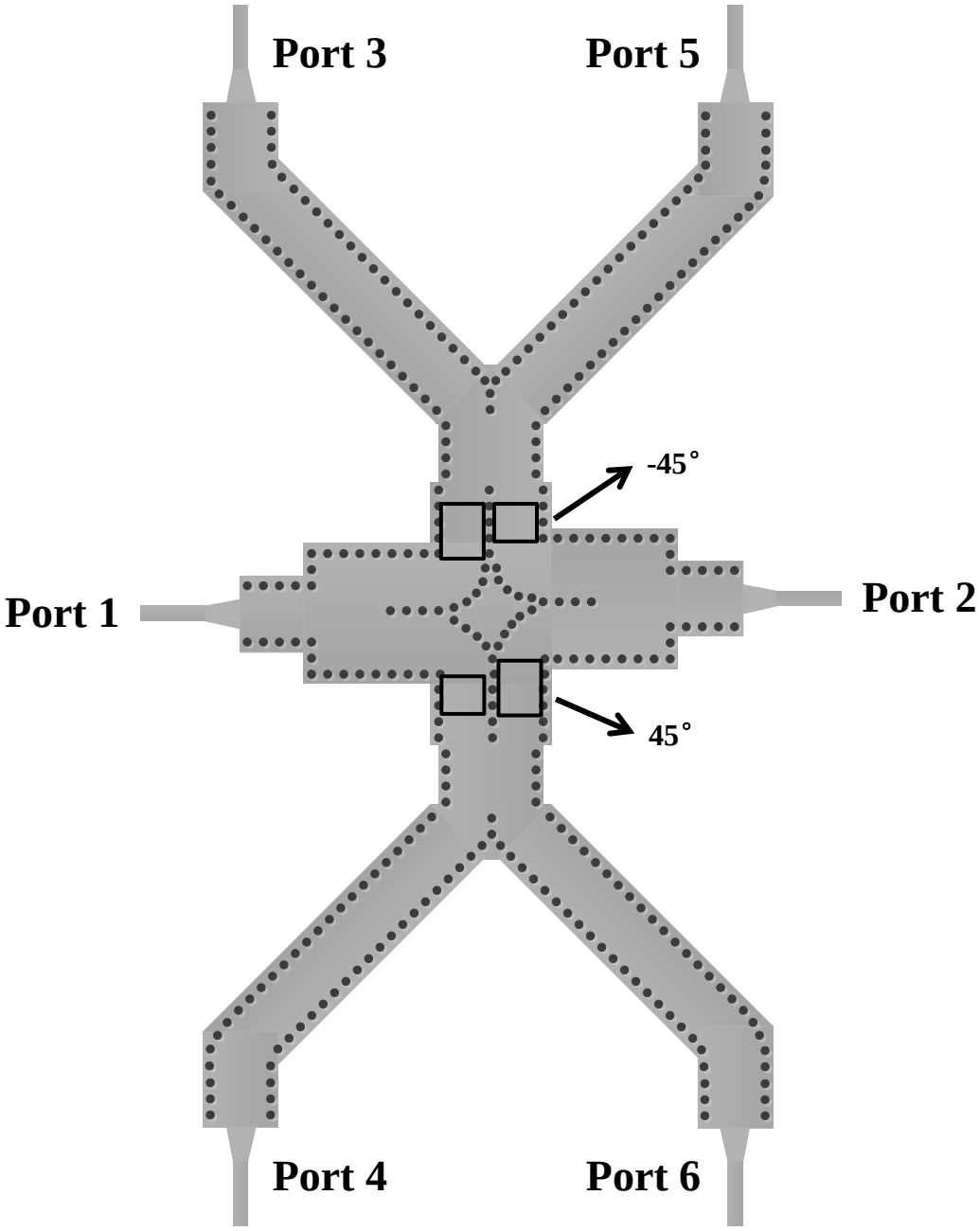

Figure 2.3 Layout of the proposed six-port circuit

The selection of the parameters that are optimized to improve the performance of the six-port circuit is based on the previous design of power divider and hybrid coupler. However, after integrating all the parts, some of the parameters (such as the step width *Ws* and the aperture length *La* of the hybrid coupler) have to be tuned again according to the following design requirement:

- Minimize the reflection coefficient S_{11} at port 1 and S_{22} at port 2, and the isolation coefficient S_{21} between the port 1 and port 2
- Keep the magnitudes of transmission coefficients S_{31} to S_{61} and S_{32} to S_{62} equal and close to -6 dB
- Keep the difference of phases between the input ports (port 1 and port 2) and the output ports (port 3, 4, 5, 6) the same as the theoretical values (see Table 2.1)

Table 2.1 Theoretical phase values of the six-port circuit

S parameter	Phase (degree)
S31	180
S41	90
S51	90
S61	180
S32	0
S42	90
S52	180
S62	90

The S-parameters simulation of the six-port is made in HFSS at center frequency 61 GHz. The final dimension of the six-port circuit is listed in Table 2.2. The simulated S parameter results are shown in Figure 2.4 ~ Figure 2.8.

Table 2.2 Dimension of the six-port circuit

Parameter	Value
ε_r	2.94
b	0.508 mm
d	0.254 mm
h	0.254 mm
a_{eqv}	2.6 mm
a	2.73 mm
L	3.8 mm
Ls	2.92 mm
Ws	0.48 mm
W	0.66 mm
Wm	1.15 mm
Lm	1.3 mm

Figure 2.4 shows magnitudes of S_{11}、S_{22} and the isolation between the two input ports (port1 to port 2) over the 60-63 GHz frequency range. It can be found that the magnitudes of S_{11} and S_{22} are better than 25 dB at the selected 60.5 GHz and better than 20 dB over the frequency range, while the isolation between these ports is 27 dB at 60.5 GHz and better than 20 dB over the frequency range.

Figure 2.5 and Figure 2.6 show the magnitudes of transmission coefficients S_{31} to S_{61} and S_{32} to S_{62} over the 60-63 GHz frequency range. It can be found that the transmission coefficients are around -6 dB at 60.5 GHz, which is very close to the theoretical values. They are located around -6 dB within an acceptable frequency range.

Figure 2.7 and Figure 2.8 show the phases of transmission coefficients S_{31} to S_{61} and S_{32} to S_{62} over the 60-63 GHz frequency range. It can be found that the phases of the transmission coefficients match the theoretical values at 60.5 GHz, which means that the $\pm 45°$ phase shifters are designed appropriately. They have a maximum error of 15 ° over the frequency range.

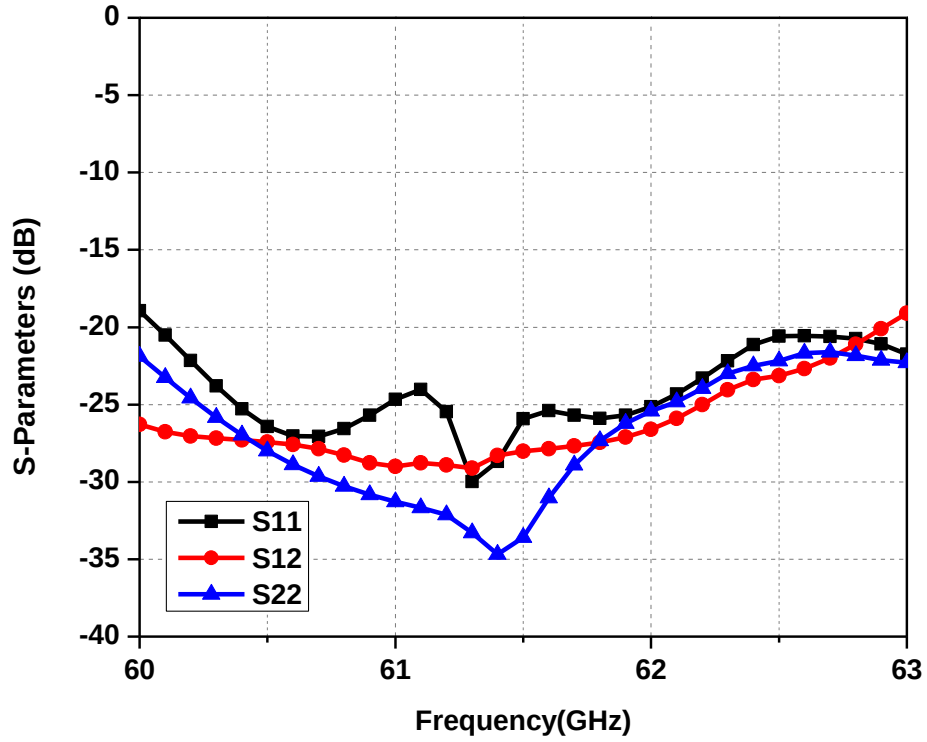

Figure 2.4 Simulated magnitudes of S_{11} 、 S_{22} and the isolation between the two input ports

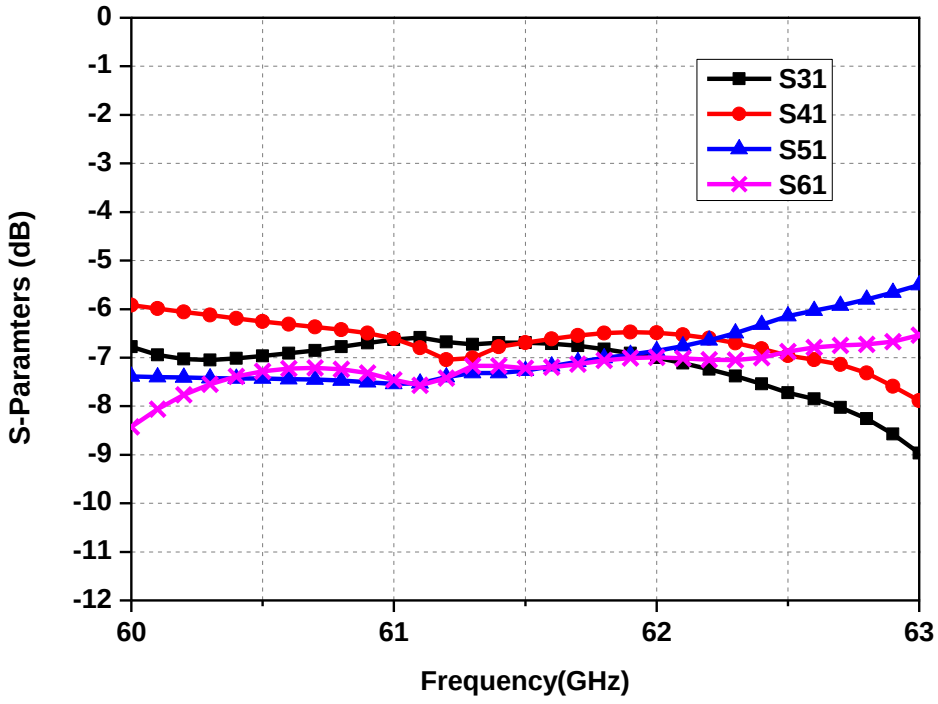

Figure 2.5 Simulated magnitudes of transmission coefficients S_{31} to S_{61}

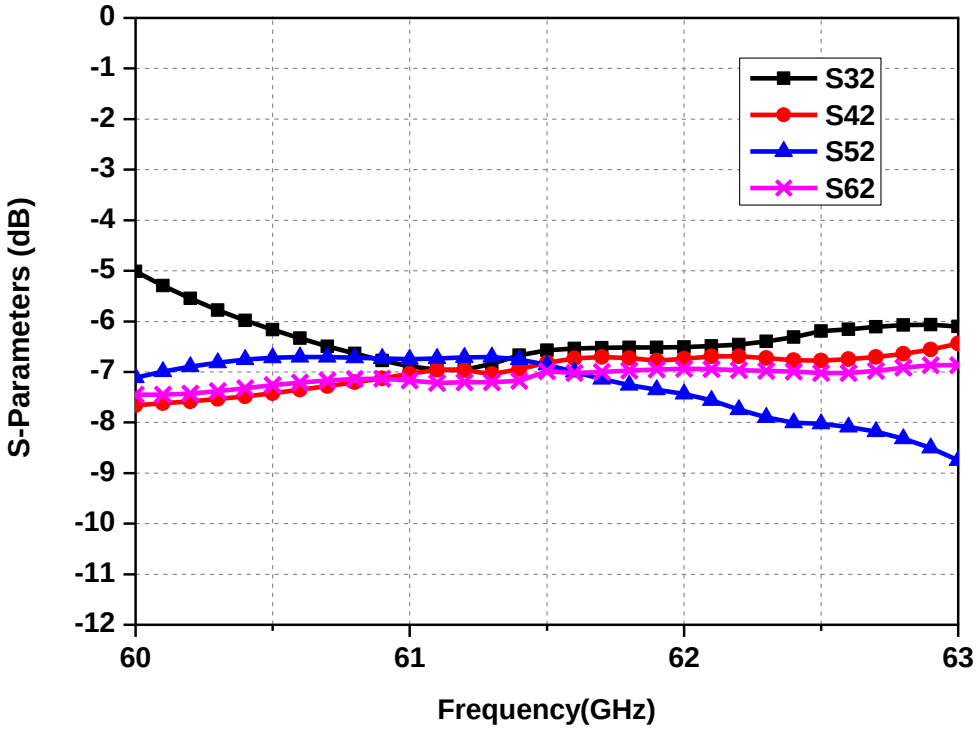

Figure 2.6 Simulated magnitudes of transmission coefficients S_{32} to S_{62}

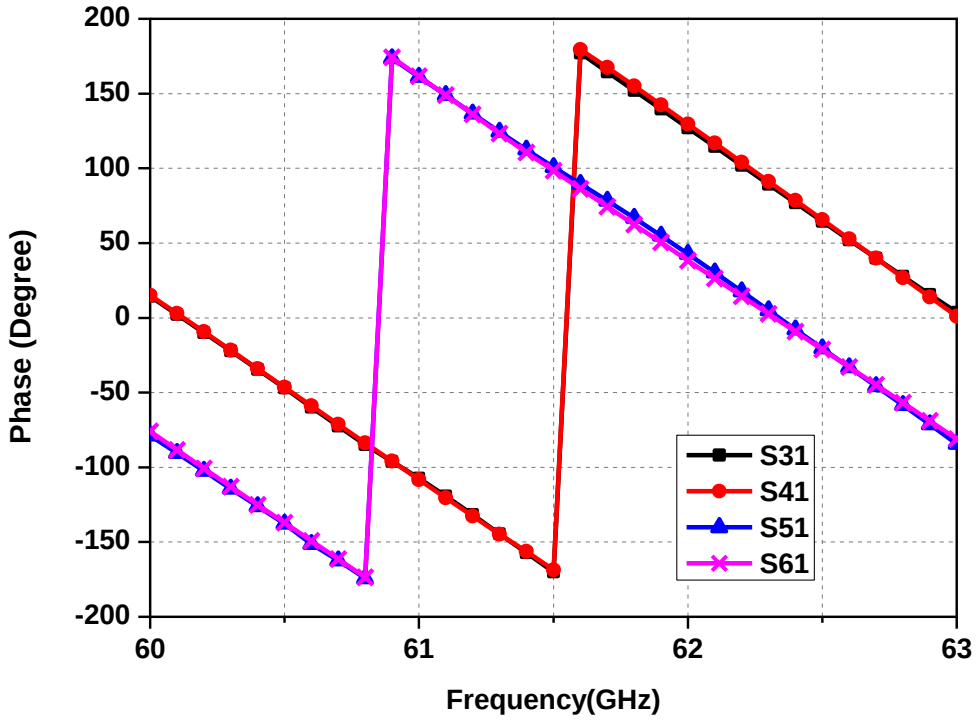

Figure 2.7 Simulated phases of transmission coefficients S_{31} to S_{61}

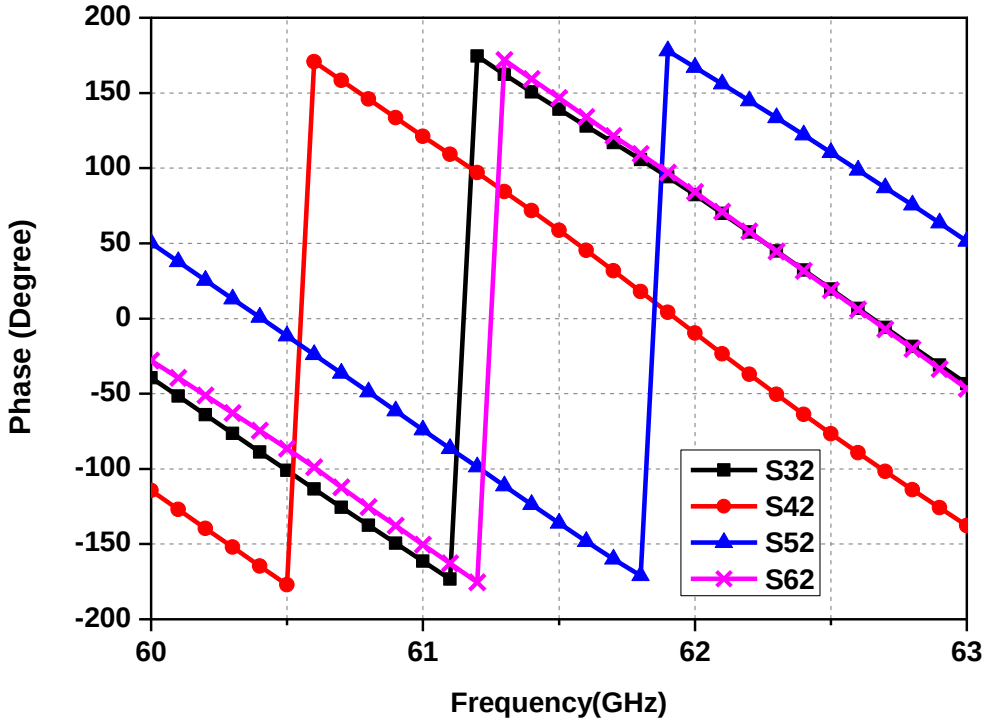

Figure 2.8 Simulated phases of transmission coefficients S_{32} to S_{62}

2.4 Measurement results of the SIW six-port circuit

The SIW six-port circuit was fabricated on a Rogers RT/duroid 6002 Laminates substrate with dielectric permittivity of 2.94 and substrate thickness of 10 mils. The total size of the six-port circuit with the transitions is 43mm × 53mm × 0.254mm.The fabrication was done by employing a laser micromachining technique which executed a complex shaped perforation. The prototype of the fabricated SIW six-port circuit and the TRL (through-reflection-line) calibration circuit are shown in Figure 2.9.

Our Anritsu 37397C network analyzer is used for S parameter measurements. V (1.85 mm) connectors (from "*Southeast Microwave*") are placed at each port of the six-port circuit for measurement purpose. The TRL calibration method is used to get rid of the influence of the SIW to microstrip line transitions by setting the reference plane after the transitions. The measurement setup of the SIW six-port circuit is shown in Figure 2.10. Measurement results are shown in Figure 2.11~Figure 2.15.

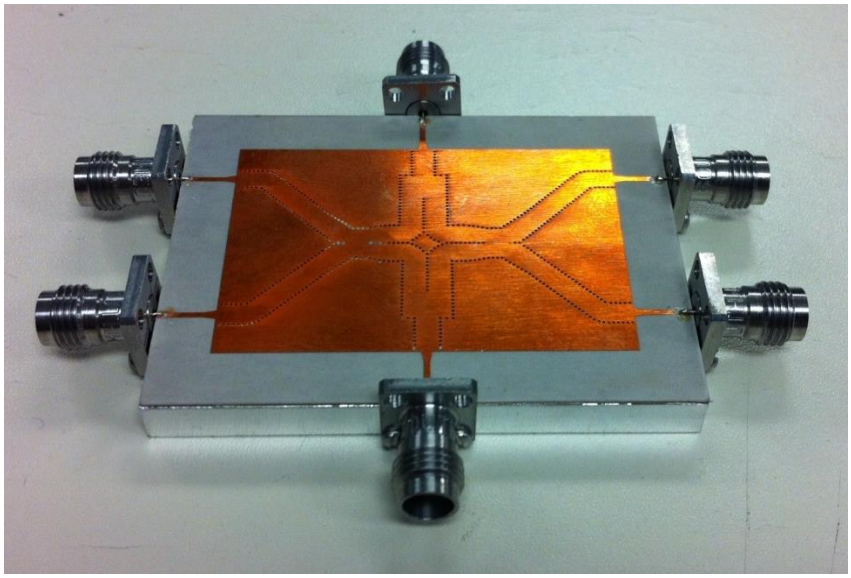

(a)

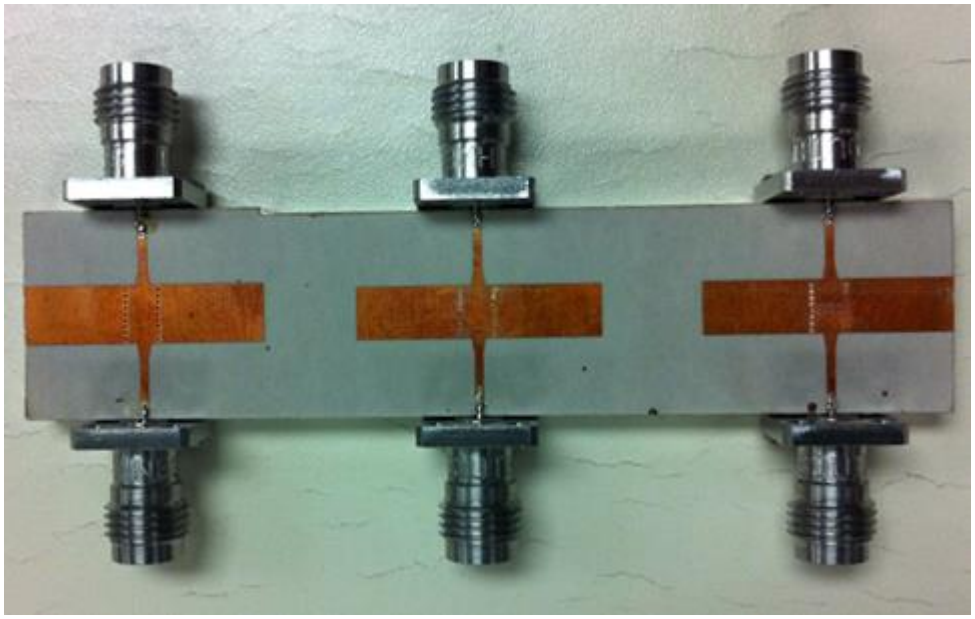

(b)

Figure 2.9 Prototype of the fabricated circuits (a) Six-port circuit (b) TRL calibration circuit

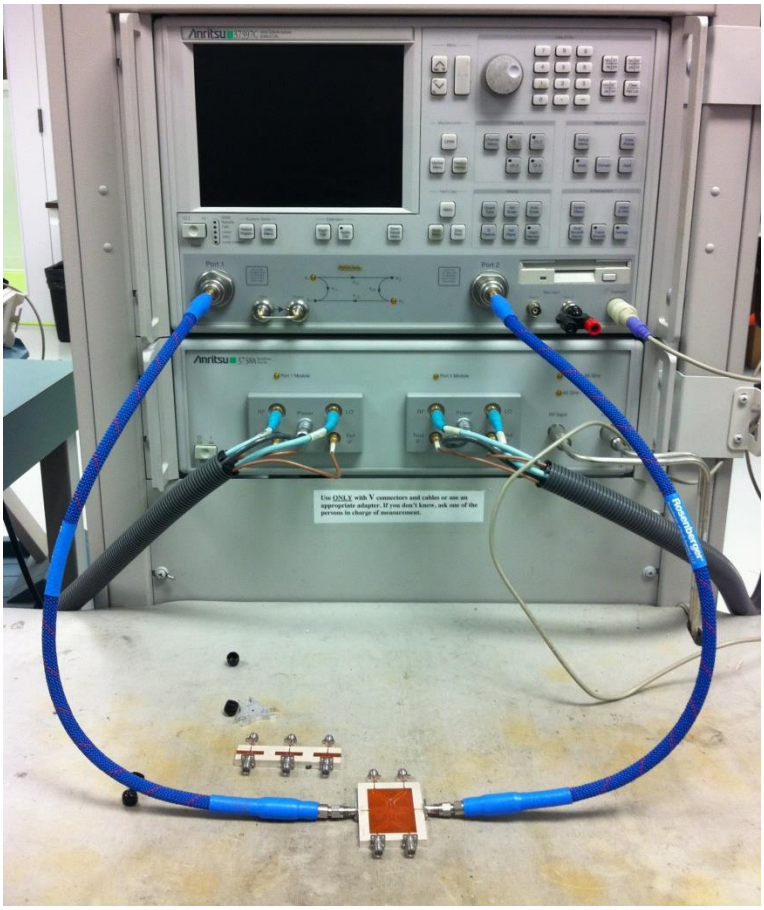

Figure 2.10 Measurement setup of the fabricated six-port circuit

Figure 2.11 shows the magnitudes of S_{11}、S_{22} and the isolation between the two input ports (port 1、port 2) over the 60-63 GHz frequency range. It can be found that the magnitudes of S_{11} and S_{22} are better than 10 dB over the frequency range, while the isolation between these ports is also better than 10 dB over the frequency range. The simulated and measured results match each other very well.

Figure 2.12 and Figure 2.13 show the magnitudes of transmission coefficients S_{31} to S_{61} and S_{32} to S_{62} over the 60-63 GHz frequency range. The transmission coefficients are around -6 dB at 60.5 GHz and within an acceptable frequency range. The simulation and measurement results agree well.

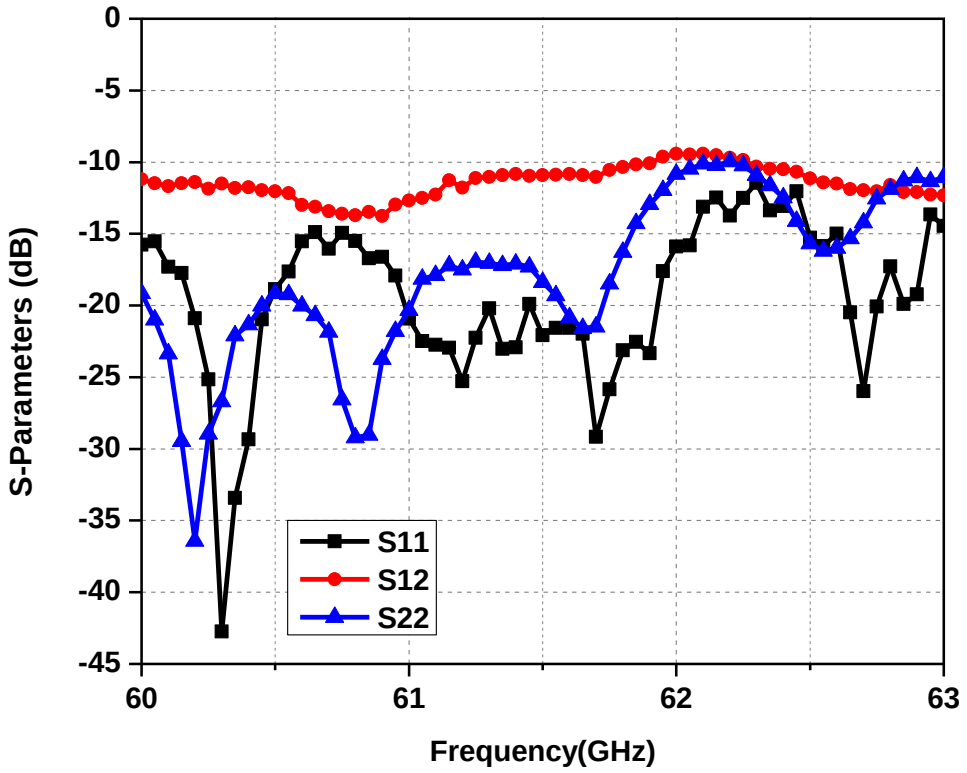

Figure 2.11 Measured magnitudes of S_{11}、 S_{22} and the isolation between the two input ports

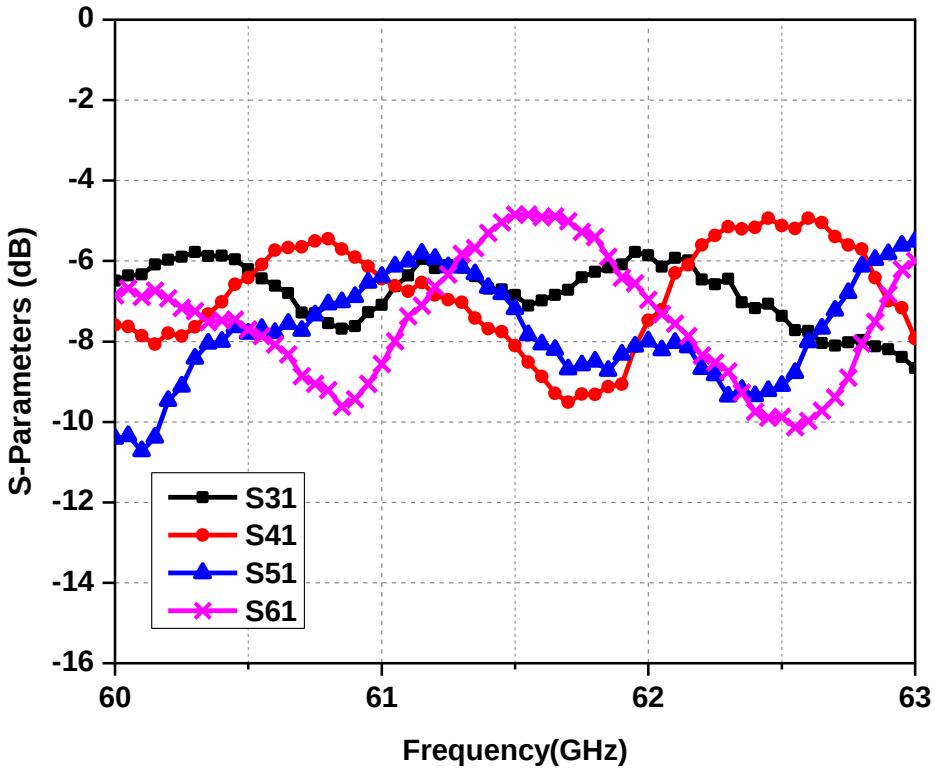

Figure 2.12 Measured magnitudes of transmission coefficients S_{31} to S_{61}

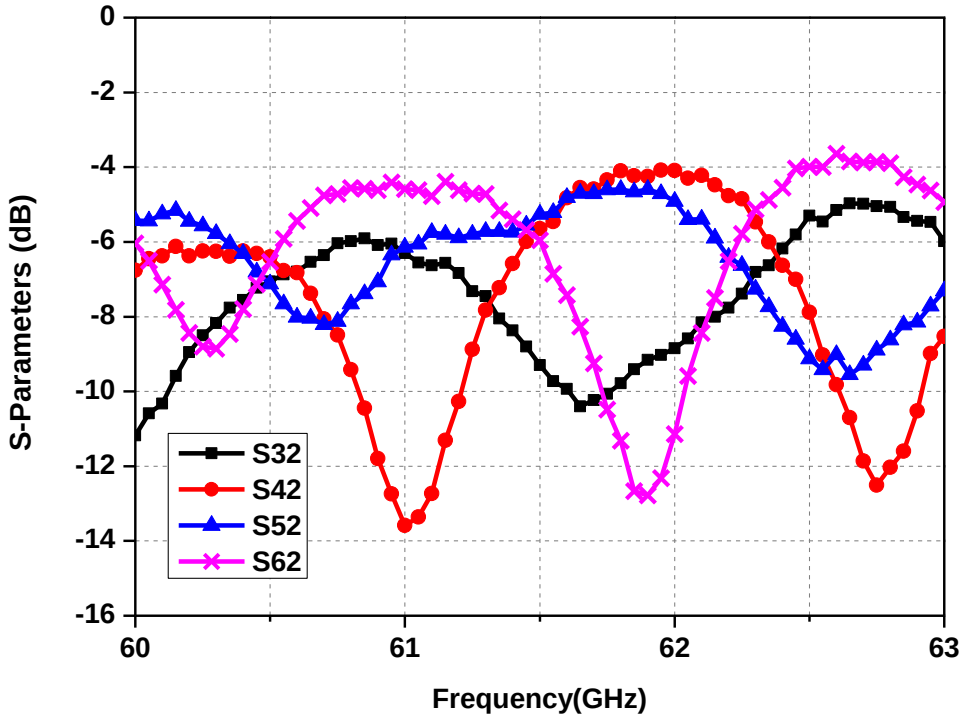

Figure 2.13 Measured magnitudes of transmission coefficients S_{32} to S_{62}

Figure 2.14 and Figure 2.15 show the phases of transmission coefficients S_{31} to S_{61} and S_{32} to S_{62} over the 60-63 GHz frequency range. It can be found that the phases of the transmission coefficients match the theoretical values at 60.5 GHz. The phase differences between S_{31} and S_{41}, S_{51} and S_{61}, S_{32} and S_{62} are close to zero, while the phase differences between S_{31} and S_{51}, S_{41} and S_{61}, S_{32} and S_{42}, S_{52} and S_{62} are close to 90 ° .

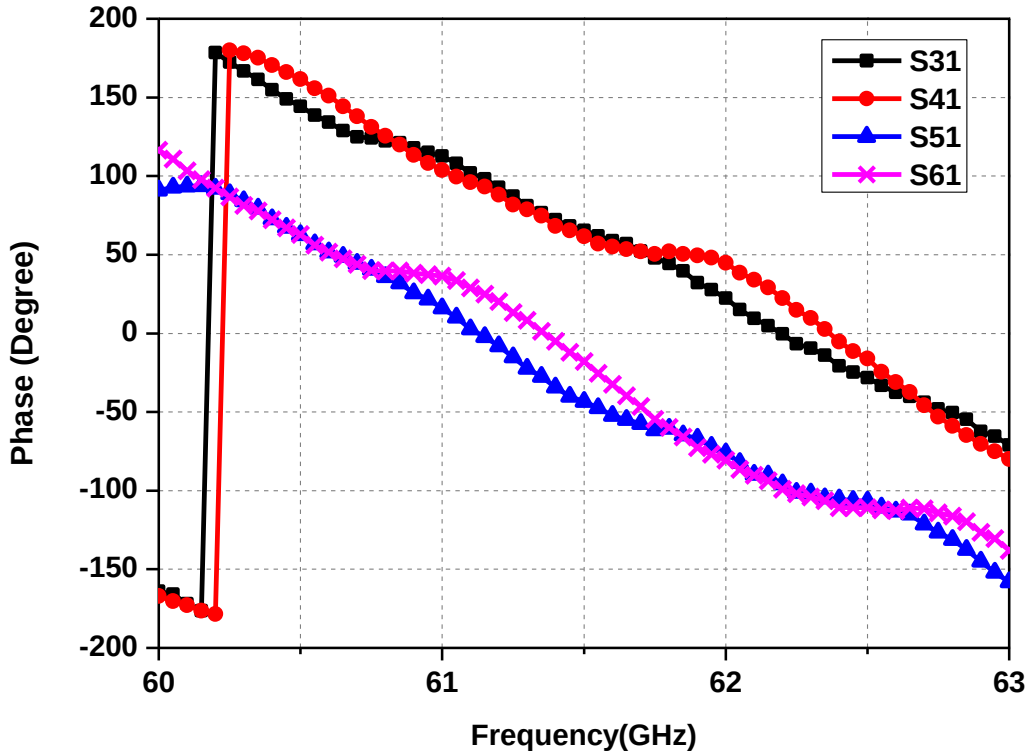

Figure 2.14 Measured phases of transmission coefficients S_{31} to S_{61}

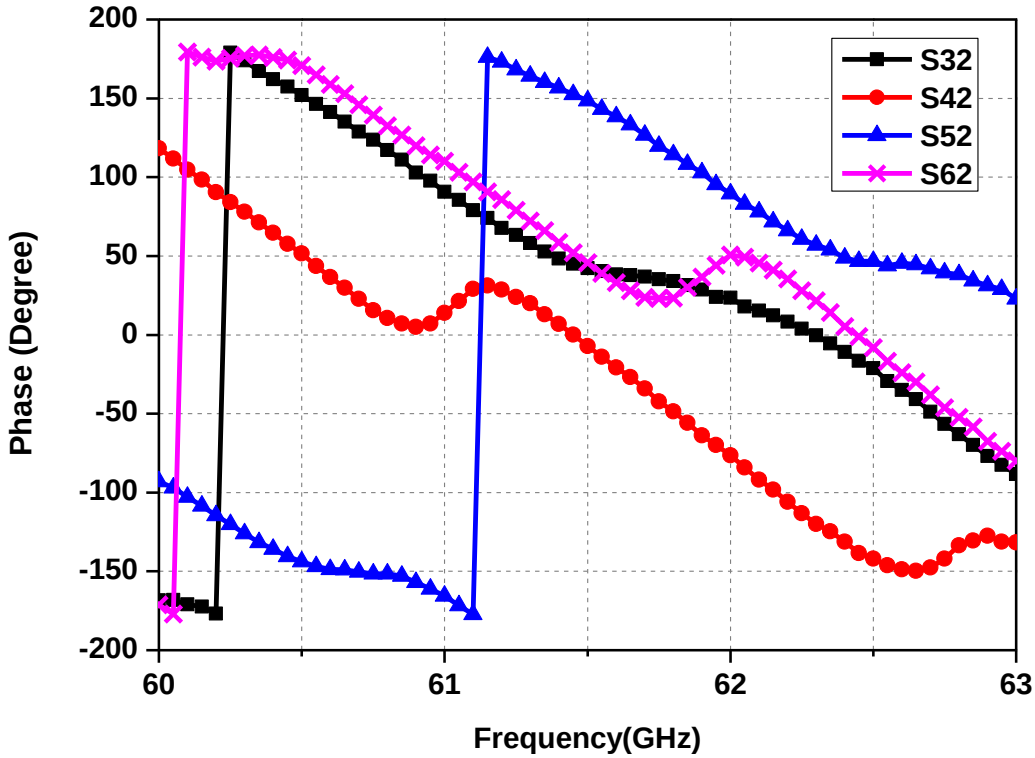

Figure 2.15 Measured phases of transmission coefficients S_{32} to S_{62}

We find out from the measurement results that the six-port circuit works well over 60-63 GHz frequency range. The next discussion will demonstrate that the fabricated six-port can support future MIMO system analysis. However, some of the curves show unexpected behaviors. The possible reasons are given as follows:

- The used V connectors are not identical. When the V connectors are connected to the six-port circuit, there is always additional effect resulting from the discontinuity between them.
- The four 50Ω loads that are connected to unmeasured ports are not good and identical. There are two male loads and two female loads, which means that additional errors could be brought to the measured phases due to the use of two transitions. Once the impedance of the loads was no longer 50 Ω, the reflection of the signals could happen at the end of the loads, resulting in deterioration of the performance of the six-port circuit. Figure 2.16 shows the changes of simulation isolation between input ports and transmission coefficients between input ports and output ports. In this case, the impedance of the loads that are connected to port 4 and port 6 is 15 Ω.
- Additional losses of the circuit during the measurement process are relatively high at 60 GHz, which makes the TRL calibration difficult to realize.

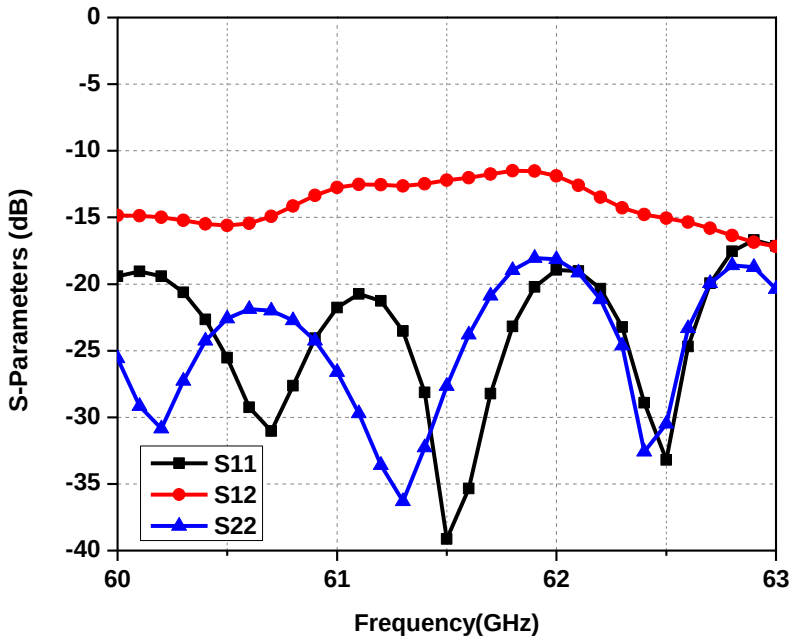

(a)

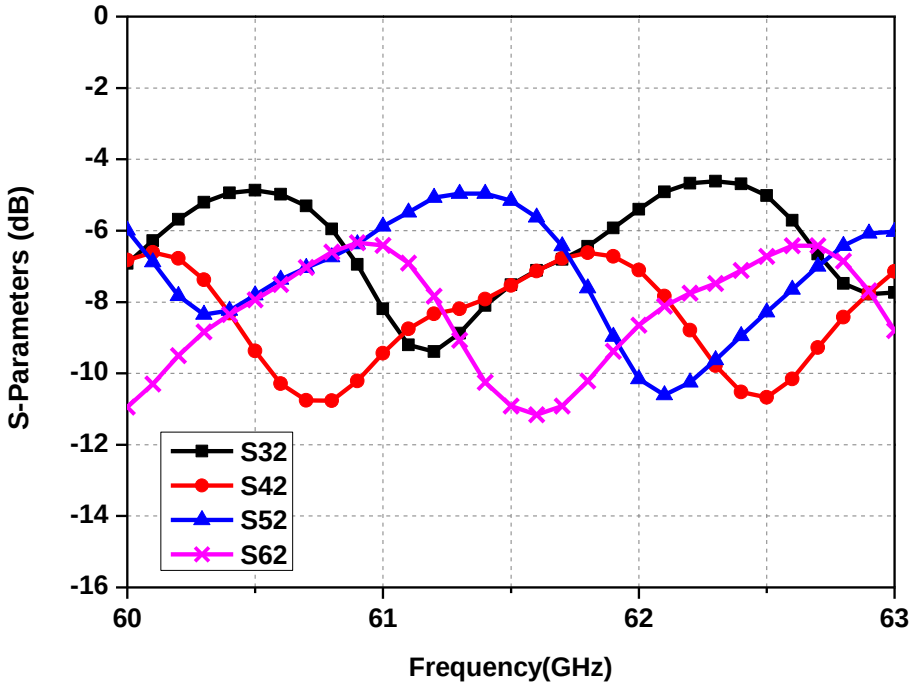

(b)

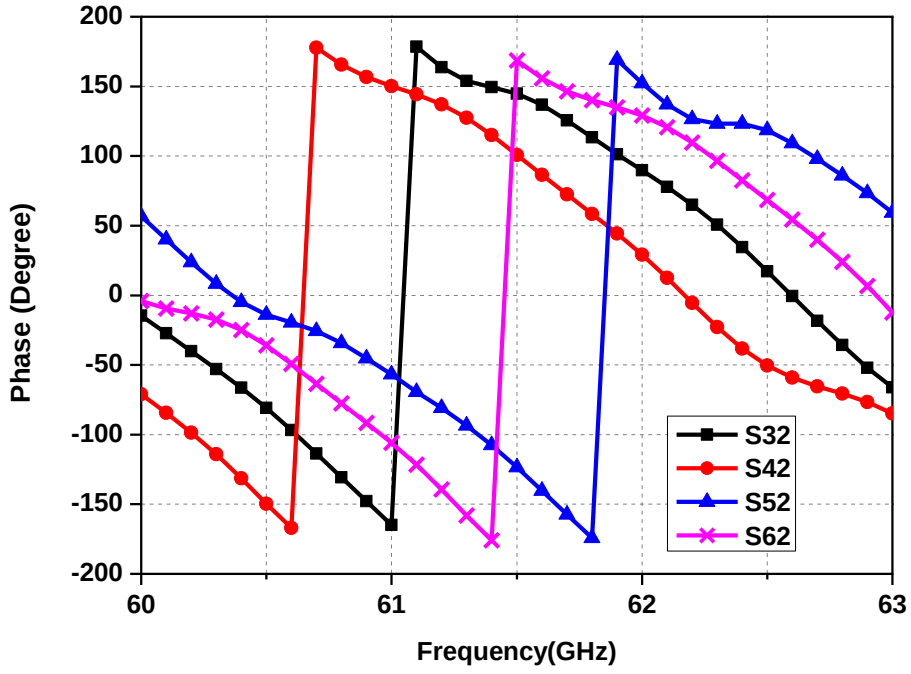

(c)

Figure 2.16 Simulation results of the six-port circuit with imperfect loads

(a) magnitudes of S_{11}, S_{22} and S_{12}; (b) magnitudes of S_{32} to S_{62}; (c) phases of S_{32} to S_{62}

2.5 Performance study of the six-port circuit for future MIMO systems

As known, the design criterion of a six-port consists of achieving a specific distribution of the q_i points. In general, a very good performance is obtained when the q_i points are equidistant from the origin and angularly spaced by 360 ºdivided their number (i = 4 in this case) [39]. When the RF and the LO ports are isolated, the q_i points of the six-port can be expressed in terms of S parameters in the following:

$$q_i = \frac{S_{i1}}{S_{i2}} \qquad i = 3, 4, 5, 6 \tag{2.13}$$

The calculation of q_i points corresponding to this design shows that they are located on the unitary circle at $exp[(2i-1)\pi/4]$. For comparison, the plots of the q_i points based on measurements from 60 GHz to 60.5 GHz are shown in Figure 2.17. As seen, the magnitudes of the q_i points are located around 1 (with maximum deviation 105.6%), while the argument difference is close to 90 ºbetween two corresponding q_i points (with maximum deviation 47.6°). The errors are produced by the measured phases of transmission coefficients S_{32} to S_{62}. In spite of this, the q_i points are located in different quadrant, which suggests that the six-port circuit can be applied in the millimeter-wave MIMO systems.

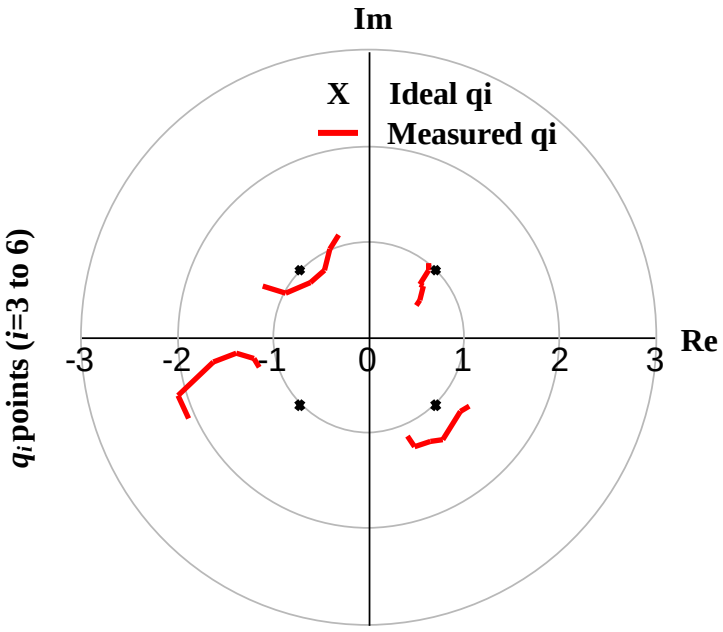

Figure 2.17 Polar plots of the measured q_i points of the proposed six-port

The six-port output voltages versus the phase differences between two RF input signals are presented in Figure 2.18. The RF source is equally split into two signals, with one of them controlled by a phase shifter. One of them is connected to the RF signal input port of the six-port circuit, while the other of them is connected to the reference signal input port.

Output voltages are shown in Figure 2.19. The output voltage minimum value points are close to 0 and shifted by 90 ° multiples. In addition, the phases of output voltages at the pairs of ports 3 and 5, 4 and 6 are opposite to each other, respectively. Therefore, I/Q output signals can be obtained by this structure.

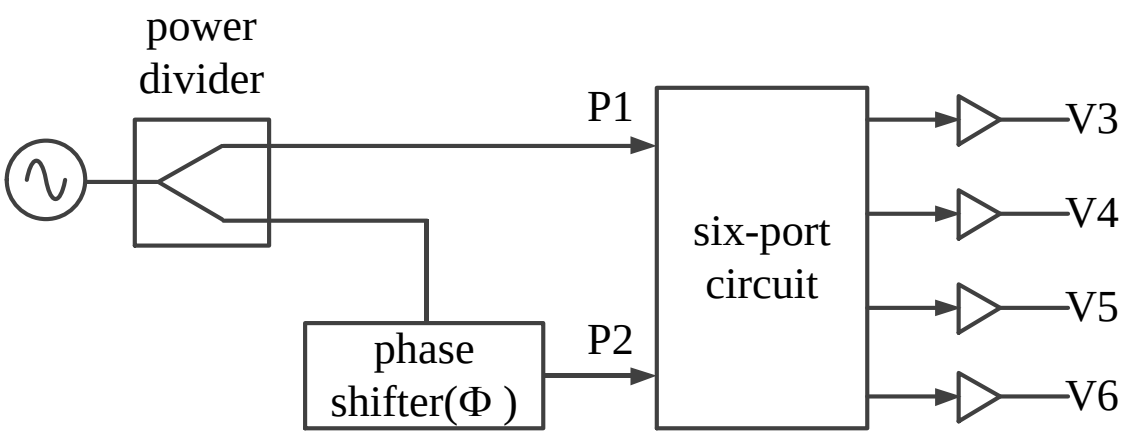

Figure 2.18 Block diagram of the six-port output voltage measurement

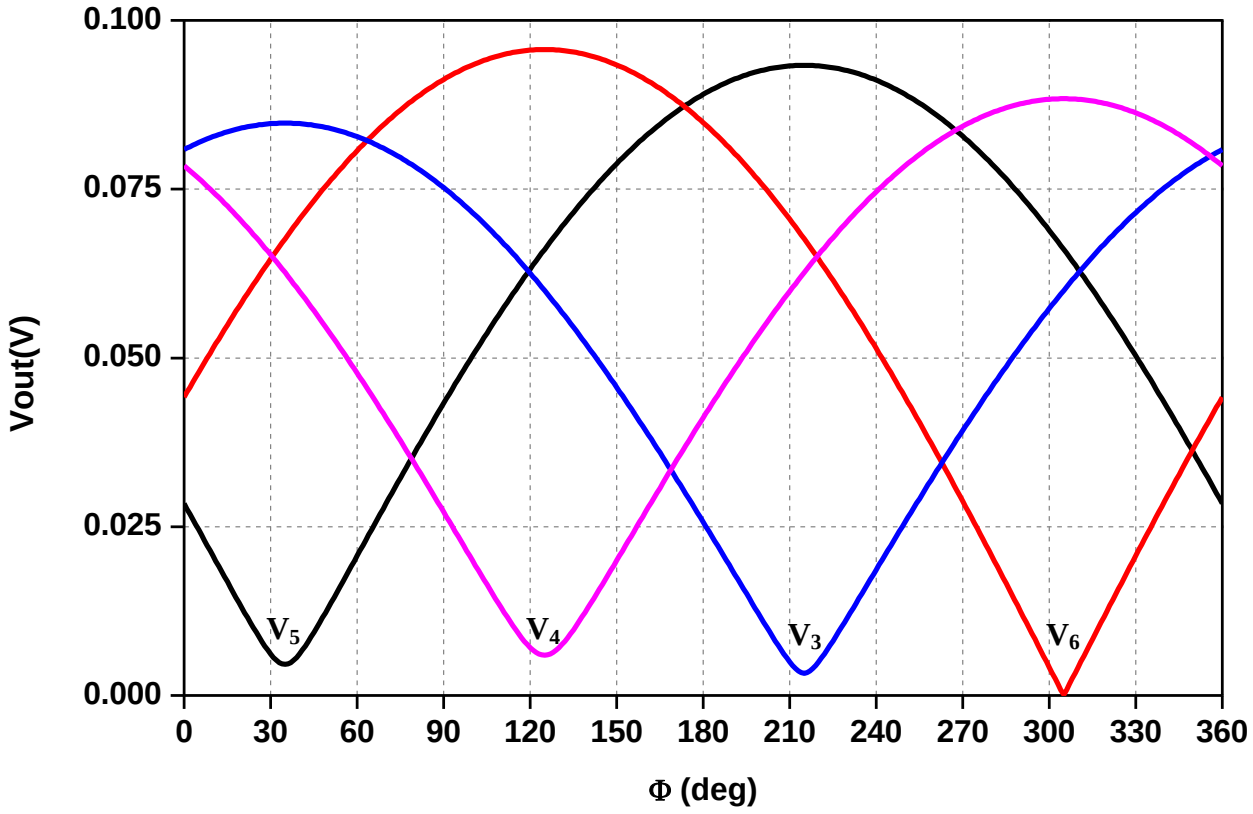

Figure 2.19 Six-port output voltages versus phase differences

The performance study of the fabricated six-port circuit has shown that it is operating well at 60.5 GHz. The distribution of q_i points and output voltage minimum positions suggest that the six-port circuit can offer good quadrature outputs that are applied in the MIMO system.

CHAPTER 3 SIX-PORT TECHNOLOGY FOR MILLIMETER-WAVE MIMO SYSTEMS

3.1 Introduction

In modern wireless communication system, the requirements for data rata are getting higher and higher. For example, more and more people are requiring huge data file transmission and real-time video streaming to support their work and entertainment that are becoming faster and faster. Recently, tens of Mbps (mega bit per second) date rate can be realized easily, while hundreds of Mbps capacities are possible with the fast developing IEEE 802.11n Wireless Local Area Network technology. However, these data rates are much lower than the 10-160 Gbps (giga bit per second) scenarios that are provided by optical links.

At the same time, millimeter-wave wireless communication is attractive for its high speed data rate to bridge the gap of channel capacity between lower frequencies and optical links. There have been published studies that realize the speed of the order of Gbps [40], [41]. For example, a 1.25 Gbps 60 GHz-band full duplex wireless Gigabit Ethernet link has been reported in [42], in which direct ASK modulation and demodulation are adopted for the transceiver. A 60 GHz MMIC chipset for radio and radar application is presented in [43], in which the data rate can reach 1 Gbps using Agilent's advanced e-beam pseudomorphic high electron mobility transistor (PHEMT) process. A 2 Gbps 60 GHz low power ultra-broadband transceiver is reported in [44], and the transceiver including antennas is fabricated in complementary metal-oxide-semiconductor (CMOS) [45]-[48] 65 nm SOI (silicon on insulator) and packaged in quad flat no-lead (QFN). Furthermore, the transceiver power efficiency is lower than 50 pJ/bit as a result of scalable power consumption that is realized by pulse generator and super regenerator oscillator architecture. A 4 Gbps 60 GHz transmission is presented in [49], in which the transmission supports the uncompressed video signal over an orbital angular momentum (OAM) wireless channel; the potential ability of spatial multiplexing based on OAM and holographic beam-forming will be a candidate for future communication. A 2 Gbps 60 GHz transmission is reported in [50], in which the channel supports the uncompressed HDTV signal by using a 60 GHz SiGe radio chipset; the baseband was equipped with both efficient random/packet error recovery and symbol-timing recovery, in order to prevent more errors in high speed data rate.

Although a high data rate transmission can be easily realized in single millimeter-wave link application, we cannot rely on it any more if the data rate keeps increasing, while the simple installation is maintained. Then, the millimeter-wave MIMO system is presented to satisfy the requirement of an extremely high data rate. On one side, conventional MIMO operating at RF and low-end microwave frequencies [51], [52] is a mature technology that makes use of multiple antennas to exploit multipath effects. On the other side, the emerging millimeter-wave MIMO is a candidate of choices to support multi-Gb/s data rate in both indoor and outdoor environments. Our purpose in this chapter is to highlight how millimeter-wave MIMO system differs from that working at lower frequencies.

The analysis of the difference between millimeter-wave MIMO systems and MIMO systems at lower frequencies can start with the Friis formula:

$$\frac{P_R}{P_T} = G_T G_R \left(\frac{\lambda_0}{4\pi d}\right)^2 \tag{3.1}$$

Where P_T is the total power from the transmitter, P_R is the received power on the receiver with its terminal impedance, G_T denotes the transmitter antenna directivity, G_R denotes the receiver antenna directivity, λ_0 is the wavelength at the working frequency, and d is the distance between the transmitter and the receiver.

In practice, the transmitter and receiver antenna directivities are stated in decibels, as are the transmitted and received powers. Then the Friis formula can be expressed in decibels as follows:

$$10\ \log_{10}\left(\frac{P_R}{P_T}\right) = G_{T,dB} + G_{R,dB} - 20\ \log_{10} f - 20\ \log_{10} d + 147.56 \tag{3.2}$$

Compared to the systems operating at lower frequencies such as 5 GHz, those operating at 60 GHz have a propagation loss of 21.58 dB or higher, for the same transmitter and receiver antenna directivity. Furthermore, compared to conventional MIMO, the millimeter-wave MIMO [53]-[54] have channels that are characterized by LoS (line-of-sight) or near LoS. Hence, spatial multiplexing can no longer be obtained through a rich scattering environment. Instead, it can be obtained by focusing the receiver antenna array on a different transmitter antenna array [55]-[57]. This is beneficial to systems which cannot make use of a spatial multiplexing deriving from the independent and identically distributed flat Rayleigh fading channels.

Millimeter-wave MIMO system has been studied in previous work. The channel modeling was studied for millimeter-wave MIMO in [58], in which two kinds of scenario were examined to observe the consequences of the MIMO LoS channels, or more generally, sparse scattering channels that have antennas with moderate separation in both indoor and outdoor environment. The results are different from the existing lower frequency MIMO systems because some special paths are dominant for the directional millimeter-wave MIMO transmission, compared to a rich scattering environment at lower frequencies. The crosstalk of the millimeter-wave MIMO system was discussed in [59], and the results demonstrated that linear MIMO crosstalk was relatively benign, as a result of being corrected by the MIMO equalizers, while nonlinear crosstalk would be much more harmful to the system that was not corrected by the MIMO equalizers. In addition, it is not feasible to realize a high precision analog/digital (AD) conversion of millimeter-wave signals by using the current technologies. Therefore, it is necessary to perform most of the signal processing to separate the data signals from different transmitters in the analog section instead of in the digital section.

The proposed system uses two six-port quadrature receivers to increase the MIMO system diversity, as explained in detail in this chapter. As it is known, the six-port is a passive circuit that acts as an interferometer; its output signals are linear combinations of phase shifted reference and input unknown signals. By using appropriate devices connected to output ports, this circuit can provide quadrature down conversion or direct modulation. The wide bandwidth, the reduced local oscillator power requirement and the very good isolation between RF inputs can be derived from its intrinsic properties.

The millimeter wave high data-rate 2 × 2 LoS MIMO wireless communication link is analyzed through Advanced Design System (ADS) software. A six-port model based on S parameter measurement of a fabricated prototype is implemented in ADS in order to obtain realistic system simulation results. In order to obtain very high data rates using a simple BPSK modulation technique on each channel, the system takes advantage of MIMO technique and fully quadrature demodulators implemented in six-port technology.

This chapter first presents the important and critical characters of the six-port circuit used to build up the 2 × 2 MIMO system, then discusses the operating principle of the entire MIMO system, applying the Rayleigh criterion to the 2 × 2 case. The 2 × 2 MIMO system architecture is shown in the next step, which is the base of the ADS simulation block diagram. Furthermore, the simulation results are shown and analyzed, including the waveforms of inputs and outputs in time domain and typical spectrums of the baseband quadrature signals. Last but not least, this chapter analyzes the BER results depending on the distance between the transmitter and receiver are shown, in the case of practical applications, when Rayleigh criterion cannot be applied, as explained later in this chapter.

3.2 System architecture and operating principle

As known, in an $N \times N$ MIMO environment, the system can be characterized by the complex channel matrix H whose normalized element h_{mn} corresponds to the channel gain from the m^{th} transmitter element to the n^{th} receiver element.

When the MIMO system operates at millimeter wave range, multipath is attenuated by high reflection losses. So we consider only the LoS component H_{LOS} of the channel response, which is shown in Figure 3.1. The channel matrix can be simplified to the LoS case:

$$h_{mn} = exp\left(j\frac{2\pi}{\lambda}d_{mn}\right) \tag{3.3}$$

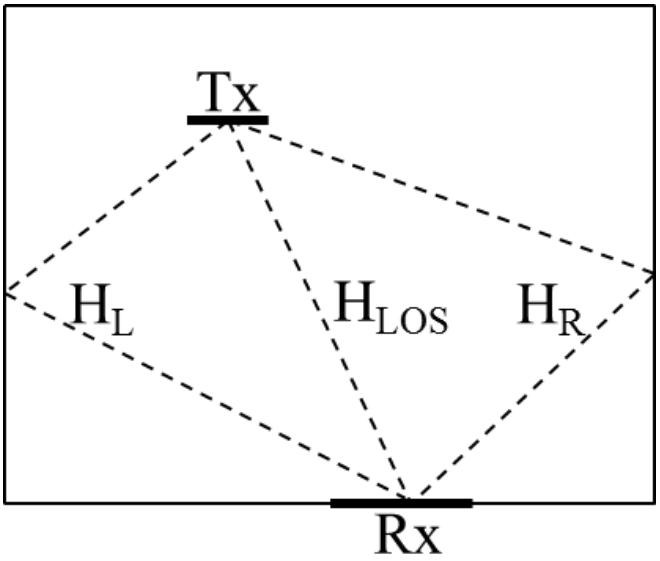

Figure 3.1 Channel response of the wireless communication system

In previous equation, d_{mn} is the path length between the m^{th} transmitter and the n^{th} receiver. We consider the case that configurations of transmitter antenna array and receiver antenna array are identical. Hence, there will be no cross-talk between two receiver array responses, if the LoS propagation Rayleigh criterion [60]-[63] is satisfied:

$$D = \sqrt{\frac{R\lambda}{N}} \tag{3.4}$$

In this Rayleigh equation, *D* is the lateral spacing of the transmitter and receiver antenna arrays, *R* is the distance between the transmitter and receiver, and λ is the wavelength of the carrier, *N* is the number of transmitters and receivers.

The columns of the channel matrix will be orthogonal:

$$H_{LoS} = [h_0,\ h_1,\ h_2 \cdots,\ h_{N-1}]$$
$$\langle h_k, h_l \rangle = 0 \tag{3.5}$$

In our proposed orthogonal system, $N = 2$ and the normalized H matrix become:

$$[H] = \begin{bmatrix} 1 & exp\left(j\frac{\pi}{2}\right) \\ exp\left(j\frac{\pi}{2}\right) & 1 \end{bmatrix} = \begin{bmatrix} 1 & j \\ j & 1 \end{bmatrix} \tag{3.6}$$

$$Rx1 = Tx1 + j \cdot Tx2$$
$$Rx2 = j \cdot Tx1 + Tx2 \tag{3.7}$$

Because of the 90° phase difference between different transmitted data, we can receive separated data after demodulation.

Figure 3.2 shows the proposed millimeter wave 2×2 MIMO six-port system architecture. In the transmitter part, two BPSK pseudo-random sequences are generated by the baseband sources, and directly modulated at millimeter-wave frequency.

The transmitter and receiver antenna arrays are identical, having the same D lateral spacing. The distance between the transmitter and receiver is R.

Various six-port architectures have been published in literature. The designs are function of fabrication technologies and specific applications: down-converter, direct modulator, or reflection coefficient measurements. The well-known six-port architecture for communication purposes is composed of two power dividers, two 90° hybrid couplers and a phase shifter as discussed in the last chapter. Unlike the other six-port circuits, this architecture can work alone without the need for any additional external loads.

The previous S-parameter measurement results have shown that the fabricated six-port is operating well at 60.5 GHz. All ports are well matched; results are better than -10 dB. The isolation between RF and LO ports (1 and 2, respectively) is at least 10 dB. The magnitudes of transmission coefficients S_{31} to S_{61} and S_{32} to S_{62} are close to -6 dB. The phases of the transmission coefficients match the theoretical values.

The six-port interferometry adds supplementary quadrature diversity to the system. A millimeter-wave direct conversion six-port based receiver, as introduced in [64], consists of a low-noise amplifier (LNA), a six-port module (SPM), and a baseband module (BBM). The SPM inputs are connected to a LNA and a local oscillator (LO), respectively.

After a square law detection using zero-bias Schottky diodes, the baseband signals are amplified by two differential amplifiers and filtered by low-pass filters (LPF). Finally, after the baseband amplifiers (BBA) amplify them, the sample and hold circuits (SHC), operating at the bit-rate frequency, generate improved quadrature output signals. Signal processing techniques are used to compensate the demodulated constellation rotation due to the inherent instability of the millimeter-wave LO.

It is obvious that, for a given D, the system will operate in an optimal condition when the distance R is identical to the calculated value according to (3.4). One of the quadrature outputs of the first receiver and the same output of the second one will demodulate different BPSK signals, BPSK_1 and BPSK_2, respectively. The other output of the receivers will demodulate the BPSK_2 and the BPSK_1, respectively.

When the distance R deviates from the optimum Rayleigh value, BER on the four outputs deteriorates, but not in identical manners. This multiple quadrature demodulation environment (spatial, due to the Rayleigh criterion, and interferometric, due to the six-port quadrature demodulator) gives the system two diversity freedom to be exploited, in order to improve the overall BER results.

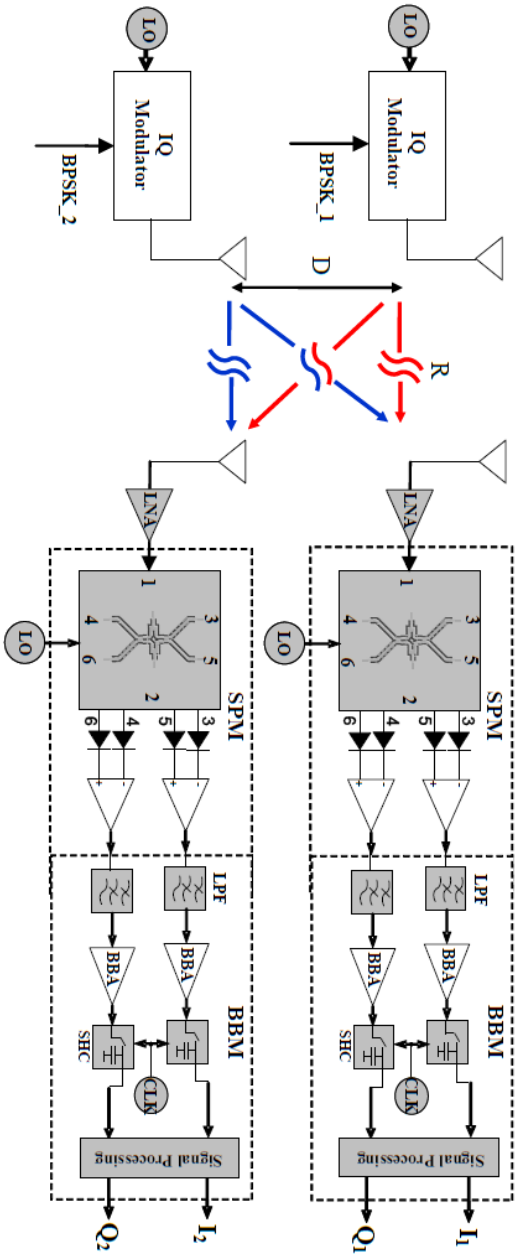

Figure 3.2 The millimeter-wave six-port based 2×2 MIMO system architecture

3.3 Demodulation results

In order to validate the proposed MIMO system, the block diagram is built based on measured six-port results at 60.5 GHz in commercial software ADS 2009, as shown in Figure 3.3. There are two BPSK modulators that transmit two different BPSK sequences. The Rayleigh criterion is realized by 2×2 antenna blocks. Two identical six-port receivers based on measured S parameter results are used to demodulate the received signals. BER is evaluated for four output combinations. They are compared to the two input BPSK sequences. The bit rate of two different BPSK pseudo-random sequences is 2 Gb/s. For a realistic lateral spacing of the 2×2 antenna arrays D = 0.1 m, the optimal distance between the transmitter and receiver is R = 4 m. According to the Rayleigh criterion, once D is changed, we can always find the optimal distance R. To calculate BER, two BPSK sequences are combined in a QPSK one. Several BERs are calculated when R is selected at the optimum of 4 m, and for two other distances (6.2 m, 8.5 m).

Figure 3.4 shows the baseband signals before the last signal processing modules that obviously improve the shape of the demodulated signals.

Figure 3.5 shows the spectrums of the modulated signal and the baseband quadrature signal. Because of the direct-conversion architecture, there is no IF (intermediate frequency) signal. The power of the modulated signal and the baseband signal are about -8 dBm and -5 dBm.

Figure 3.6 and Figure 3.7 show the waveforms of the inputs and outputs in time domain for the ideal (R = 4 m) case. For either input sequence, there are two identical output sequences that are the same as the input one, as a result of the inherent MIMO spatial and additional quadrature diversity (due to six-port interferometry).

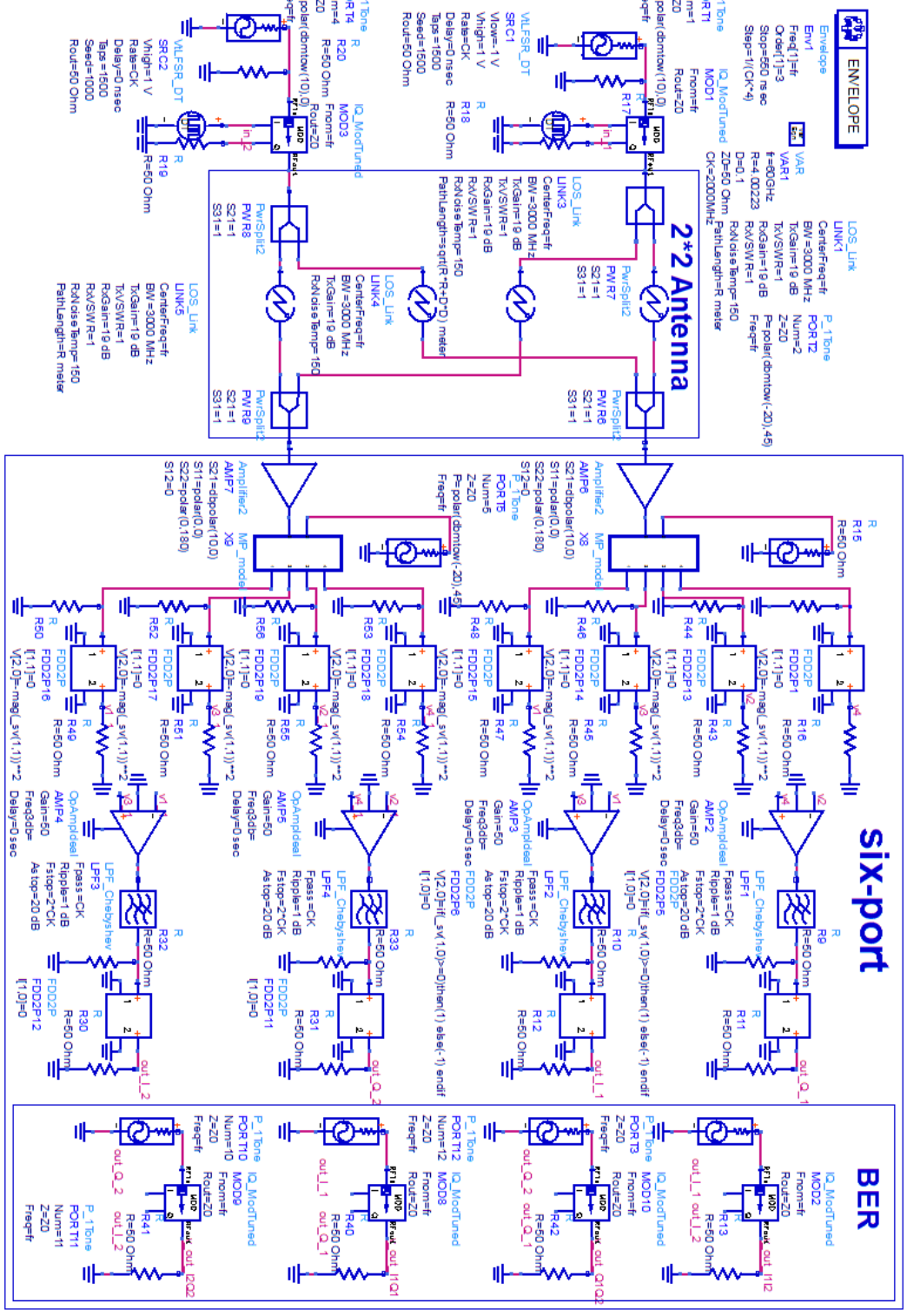

Figure 3.3 Block diagram of the proposed 2×2 MIMO system

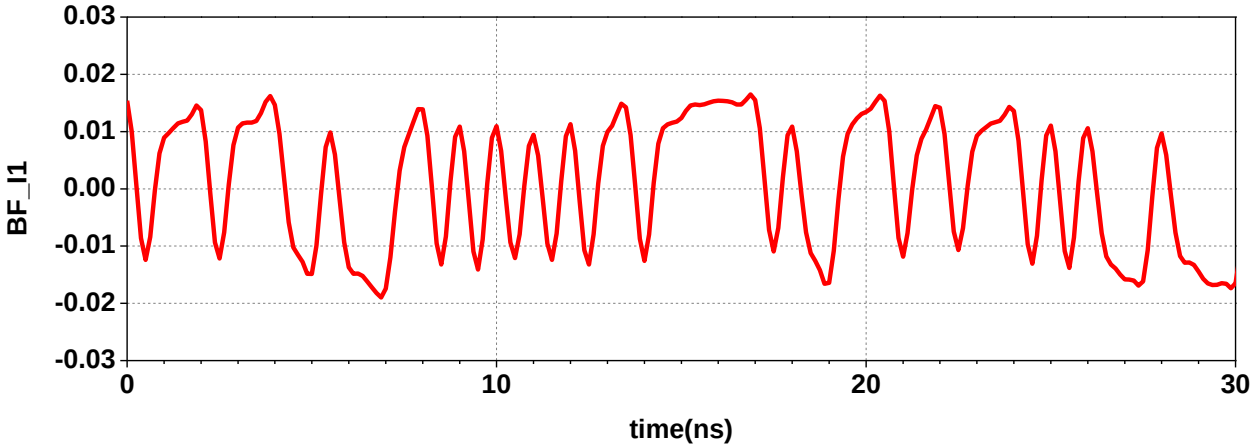

(a)

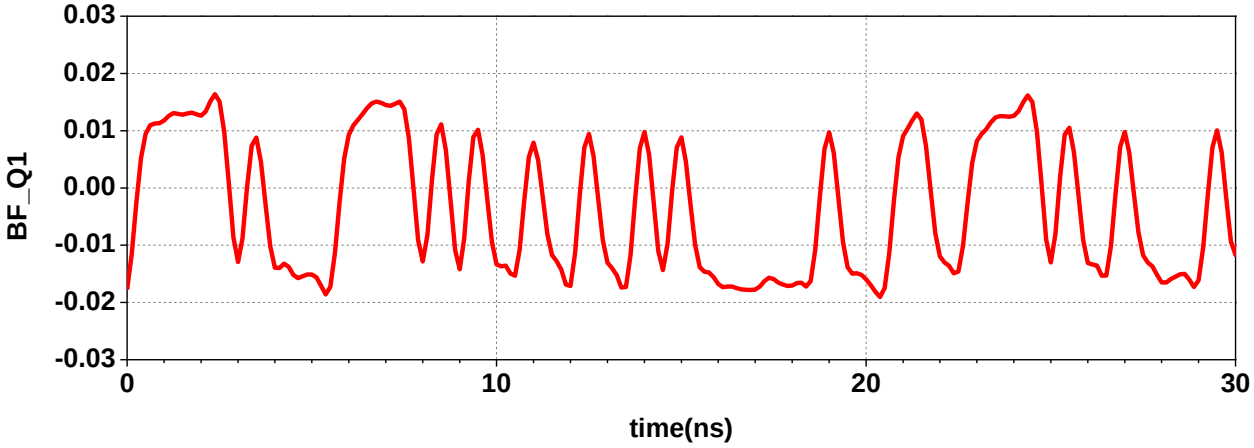

(b)

Figure 3.4 Waveforms of the baseband signals before the signal-shaping module (a) I signal; (b) Q signal

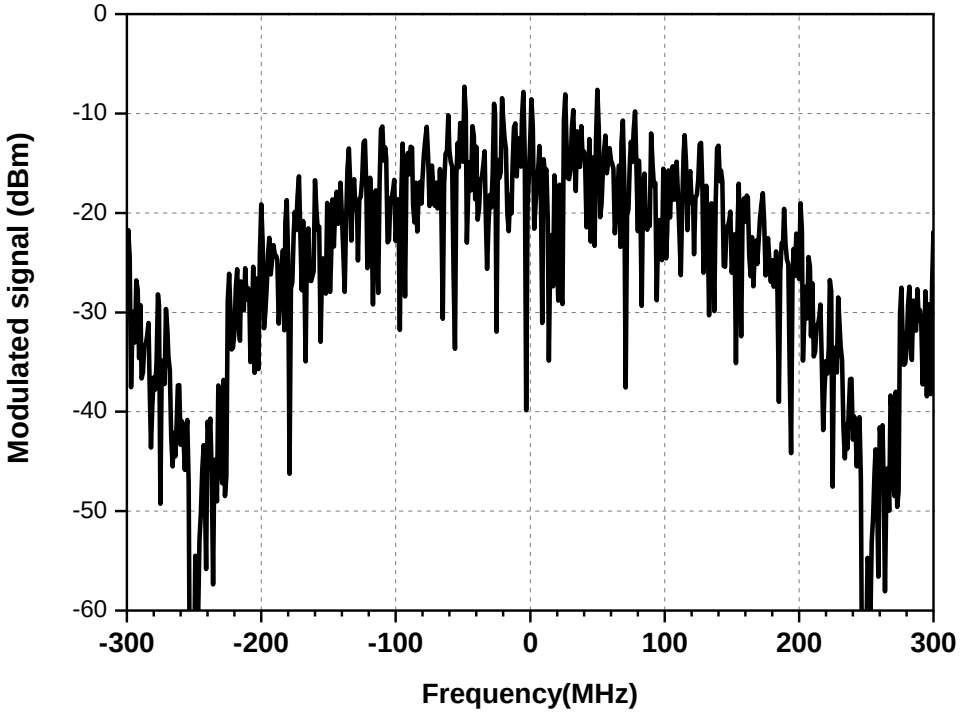

(a)

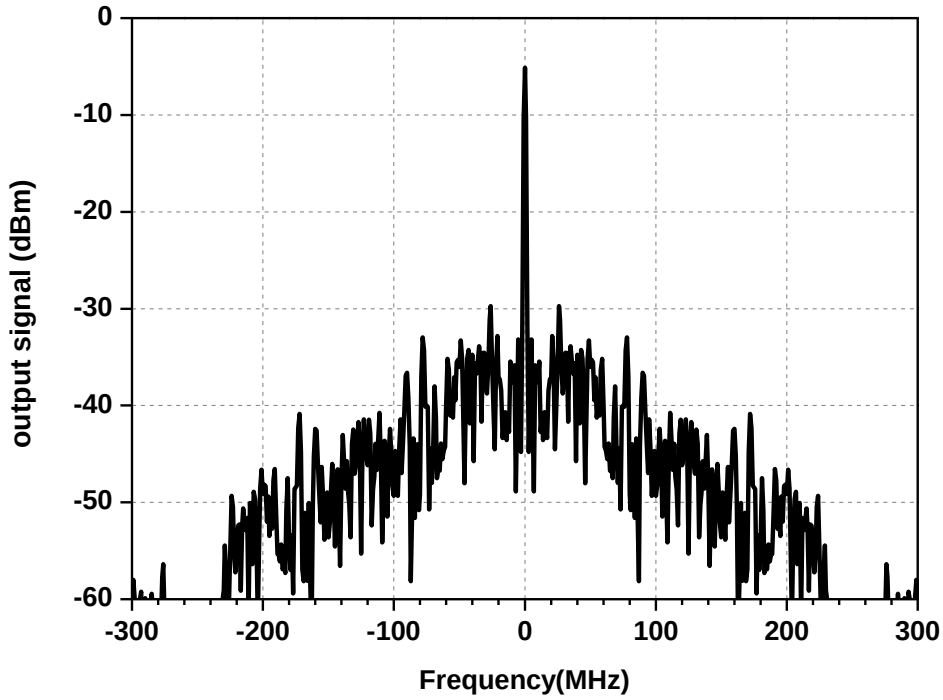

(b)

Figure 3.5 Spectrums of the modulated signal and the baseband signal (a) the modulated signal; (b) the baseband signal

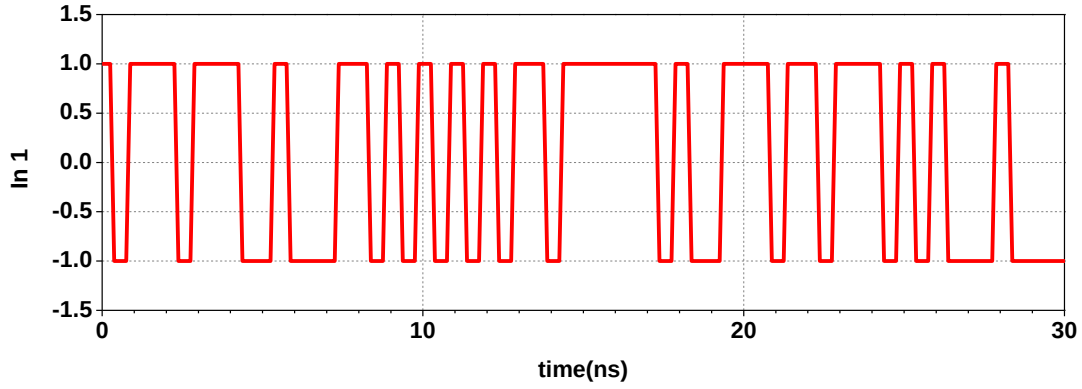

(a)

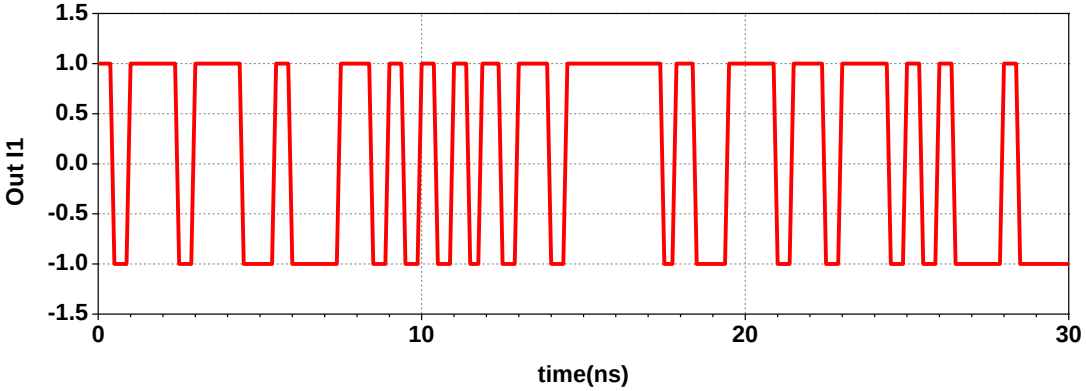

(b)

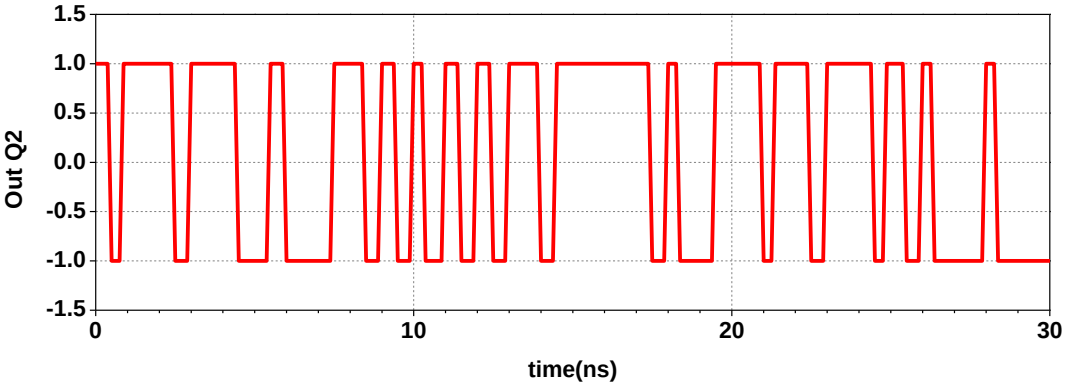

(c)

Figure 3.6 Waveforms of the first input and output signals

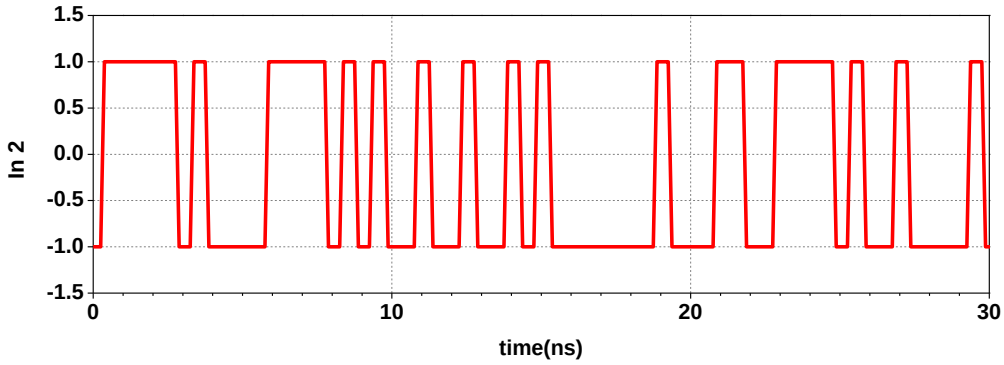

(a)

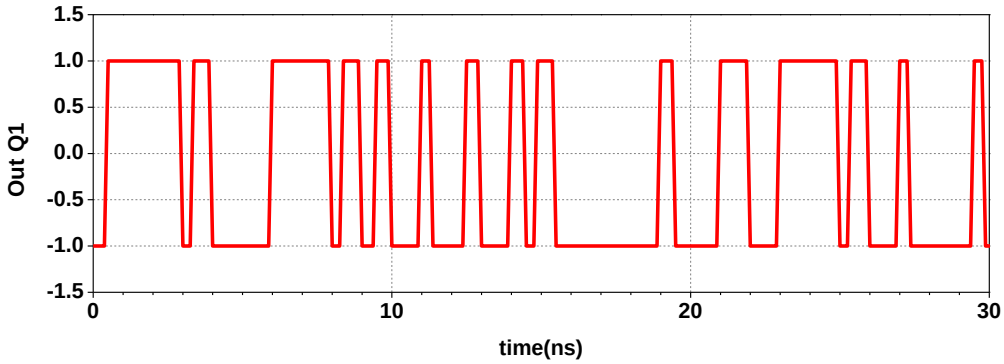

(b)

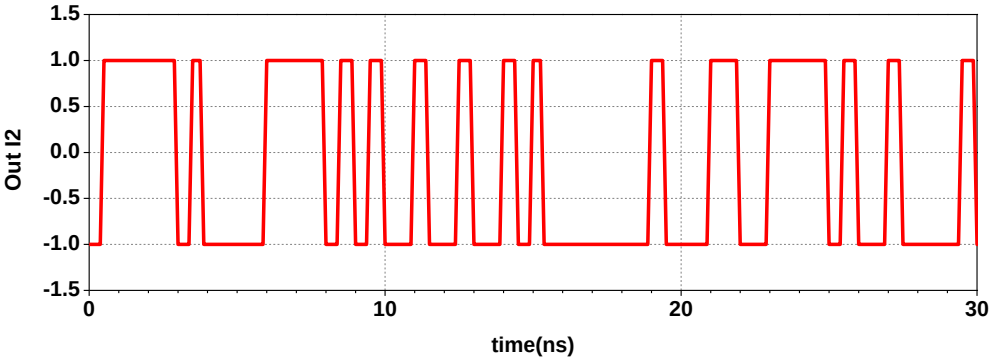

(c)

Figure 3.7 Waveforms of the second input and output signals

Figure 3.8 shows the simulated BER as a function of the average energy of a modulated bit to noise power spectral density ratio (E_b/N_0), when the distance between the transmitter and receiver is optimal, R = 4 m. It can be seen that the BER of four different pairs of demodulation results (I_1I_2, Q_1Q_2, I_1Q_1, and I_2Q_2) are identic al and superposed with the ideal BPSK/ QPSK value. The BER are less than 1.0E^{-6} once the E_b/N_0 ratio is higher than 10.8 dB. The reason is that, when the distance R = 4 m, the Rayleigh criterion is satisfied. There is no cross-talk between two BPSK uncorrelated sequences.

The simulated BER is based on the formula that is used to calculate the efficiency of the receiver:

$$P_e = \frac{1}{2} erfc \sqrt{\frac{E_b}{N_0}} \tag{3.8}$$

$$\text{erfc}(x) = \frac{2}{\sqrt{\pi}} \int_x^{\infty} exp^{-w^2} dw \tag{3.9}$$

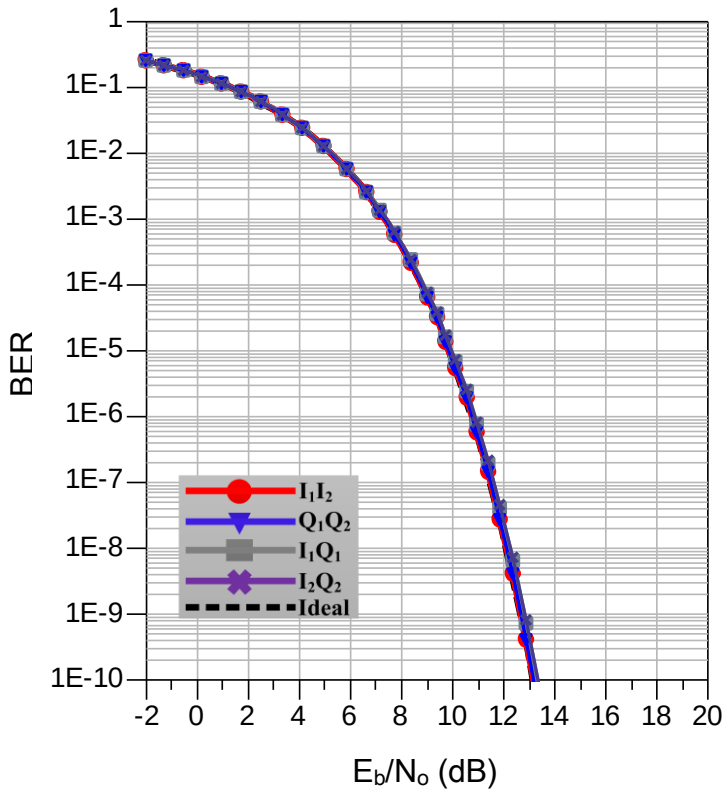

Figure 3.8 Simulated BER versus E_b/N_0 for optimum R=4 m

Figure 3.9 shows the simulated BER when the distance is increased by around 50%, at R = 6.2 m. As can be seen, the lowest BER can be easily selected from the four plotted values. In this case, the best result comes from the I_1I_2 output pair; the BER is less than 1.0E^{-6} once the E_b/N_0 ratio is higher than 11.4 dB.

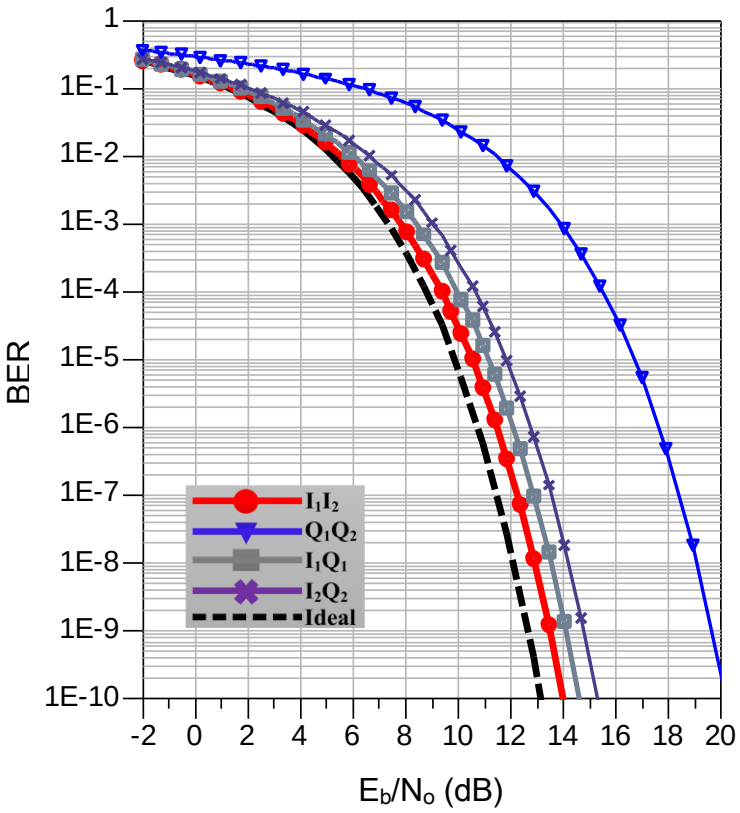

Figure 3.9 Simulated BER versus E_b/N_0 for R=6.2 m

Figure 3.10 shows the simulated BER when R = 8.5 m, close to maximum range for such indoor systems (R = 10 m). It can be seen that the optimal output pair is changed from I_1I_2 to I_2Q_2; the BER value is less than 1.0E^{-6} once the E_b/N_0 ratio is higher than 11.6 dB.

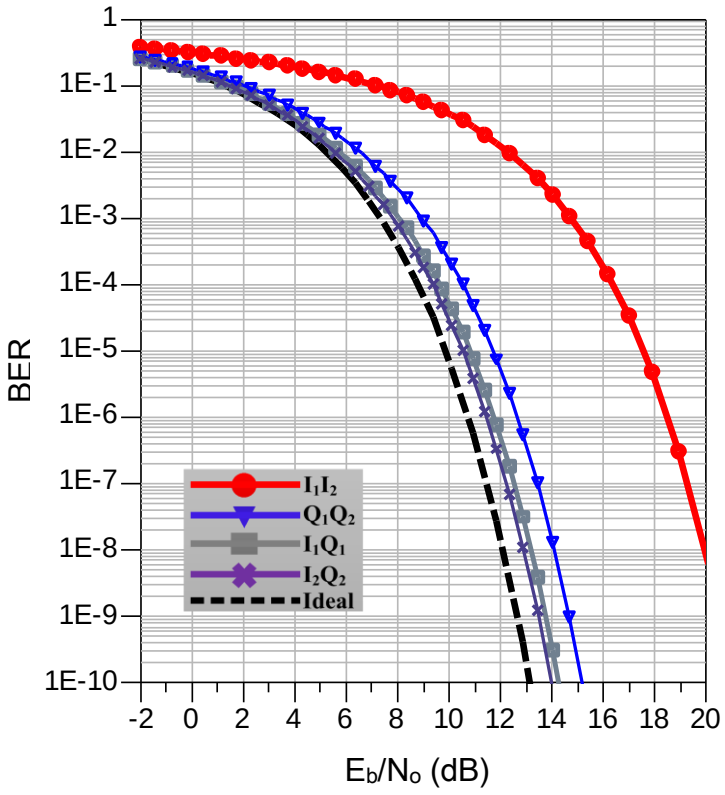

Figure 3.10 Simulated BER versus E_b/N_0 for R=8.5 m

In the last two cases, because R is different from the ideal value, there is a cross-talk between BPSK sequences. However, from the above BER results, we can always find an optimum pair of outputs to minimize the BER.

As suggested earlier, a practical V-band indoor communication system operates over less than 10 m range using portable devices. The D value can be initially chosen for intermediate range of around R = 4 m, corresponding at D = 0.1 m, a realistic value for today's transceiver dimensions. The analysis can be done individually evaluating each BER value with a known pseudo-random bit sequence. The pair of signals having the best BER will be chosen for each different R distance. It is to be noted that for fixed configurations, when R is unchanged, the distance D between antennas will be chosen according to the LoS Rayleigh criterion.

Figure 3.11 shows the demodulation results of a QPSK signal. All clusters remain well positioned after the signal processing module in the I/Q complex plane.

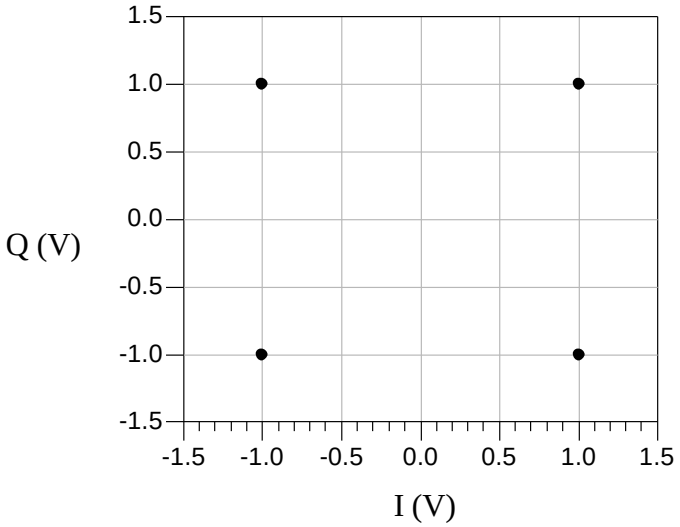

Figure 3. 11 Constellation of demodulated QPSK signal

3.4 Conclusion

In this chapter, a millimeter wave 2 × 2 MIMO system based on six-port technology is proposed and validated through advanced system simulations.

In order to obtain realistic simulation results, the six-port circuit model is based on S-parameter measurement on a fabricated circuit. The measured S-parameters exhibit very good amplitude and phase balance in the considered frequency band, between 60 and 63 GHz, while maintaining a high isolation and good matching for the RF inputs.

BER results of the proposed 2 × 2 MIMO system show that an optimum output quadrature pair can be selected among the four available combinations, depending on the range, if the Rayleigh criterion is not strictly applied.

The use of the quadrature six-port demodulator in each receiver instead of a simple BPSK demodulator provides an additional degree of freedom for the proposed MIMO system, fully exploited in this analysis. Hence, the system ensures improved BER as compared to a Single-Input Single-Output (SISO) one, depending on the distance between the transmitters and receivers.

CONCLUSION

The millimeter-wave MIMO system based on SIW six-port technology is presented and validated in this dissertation. This wireless communication system can support multi-Gbps data transmission, which is necessary for modern home or office wireless network and entertainment. BER results of the proposed 2 × 2 MIMO system show that one optimum output quadrature pair can be selected among the four available combinations, depending on the range between the transmitter and the receiver, compared to a Single-Input Single-Output (SISO) one, once the Rayleigh criterion is not strictly satisfied. The other results, including the spectrums of the modulated signal and the baseband quadrature signal and the waveforms of the inputs and outputs in time domain ensure that the system is working in the appropriate way. The use of the quadrature six-port demodulator in each receiver instead of the common BPSK demodulator provides an additional degree of freedom for the proposed 2 × 2 MIMO system.

Before the final millimeter-wave 2 × 2 MIMO system is presented, several basic techniques are deep discussed and analyzed in advance. All of them make it possible to design and validate the MIMO system:

- SIW technology and its application in the design and development of power dividers and hybrid couplers

  The SIW structure is chosen to design the fundamental components of the six-port circuit because of its low cost, low insertion loss, high power capability and easy integration with planar circuits. The SIW power dividers and hybrid couplers are analyzed and designed.

  The simulation results show that all the ports of the power dividers and hybrid couplers are matched (at least -20 dB over the desired frequency band). The magnitudes of the transmission coefficients are close to -3 dB.

- Six-port technology

  The quadrature down-conversion of the six-port circuit makes it an excellent candidate of the proposed millimeter-wave MIMO system. The simulation and measurement results agree well.

The S-parameter measurement results have shown that the fabricated six-port is operating well at 60.5 GHz. All ports are well matched; results are better than -10 dB. The isolation between RF and LO ports (1 and 2, respectively) is at least 10 dB. The magnitudes of transmission coefficients S_{31} to S_{61} and S_{32} to S_{62} are close to -6 dB. The phases of transmission coefficients match the theoretical values.

- Millimeter-wave MIMO system

  Millimeter-wave MIMO systems can provide high speed data rate, which differ from those at lower frequency bands. Rayleigh criterion should be satisfied in order to eliminate crosstalk between two receiver array responses.

  The performance of the millimeter-wave MIMO system depends on the measurement results of the six-port circuit. The output voltages versus the phase differences between two RF input signals show that the output voltage minimum value points are shifted by 90° multiples. Therefore, I/Q output signals can be obtained by this structure.

The millimeter-wave 2×2 MIMO system based on the SIW six-port technology opens the way to low-cost reliable high-speed communication systems. The combination of the millimeter-wave MIMO technology and the six-port technology allows a novel solution to the high data rate requirement in modern wireless communication system. This kind of solution could be available for future MIMO systems that are more complicated and require higher date rate, such as millimeter-wave 3×3 and 4×4 MIMO systems.

REFERENCES

[1] *Federal Communications Commission* (*FCC*) Part 15.255 (57 - 64 GHz unlicensed band), May 2000.

[2] *Federal Communications Commission* (*FCC*) Docket 05 - 45 (71 - 76 GHz, 81 - 86 GHz, 92 - 95 GHz), March 2005.

[3] F. D. L. Peters, S. O. Tatu, T. A. Denidni, "Design of Traveling-Wave Equidistant Slot Antennas for Millimeter-Wave Applications", accepted to *2011 IEEE AP-S,* Spokane, WA, July 3 - 8, 2011.

[4] G. Brehm, "Trends in Microwave/Millimeter-Wave Front-End Technology", *1st EuropeanMicrowave Integrated Circuits Conference*, pp. 1 - 4, Manchester, September 10 -13, 2006.

[5] C. Park, T. Rappaport, "Short-Range Wireless Comm. for Next-Generation Networks: UWB, 60 GHz Mm-wave WPAN and ZigBee", *IEEE Wireless Comm.*, vol. 14, pp. 70 - 78, August 2007.

[6] A.M. Niknejad, "Siliconization of 60 GHz", *IEEE Microwave Magazine*, vol.11, no. 1, pp. 78 - 85, February 2010.

[7] A. Forenza, RW. Heath Jr., "Benefit of Pattern Diversity via Two-Element Array of Circular Patch Antennas in Indoor Clustered MIMO Channels." *IEEE Transactions on Communications*, vol. 54, no. 5, pp. 943 - 954, May 2006.

[8] D. Piazza et al., "Design and Evaluation of a Reconfigurable Antenna Array for MIMO Systems," *IEEE Transactions on Antennas and Propagation*, vol. 56, no. 3, pp. 869 - 881, Mars 2008.

[9] A. Grau, H. Jafarkhani, F. De Flaviis, "A Reconfigurable MIMO Communication System," *IEEE Transactions on Wireless Communications*, vol. 7, no. 5, pp. 1719 - 1733, May 2008.

[10] J.F. Frigon, C. Caloz, Y. Zhao, “Dynamic Radiation Pattern Diversity (DRPD) MIMO Using CRLH Leaky-Wave Antennas,” in *Proc. RWS 2008*, Orlando, FL, January 2008.

[11] X. Li, J.F. Frigon, “Capacity Analysis of MIMO Systems with Dynamic Radiation Pattern Diversity”, in *Proc. VTC – Fall 2009*, pp. 1 - 4, Barcelona, Spain, April 2009.

[12] F. Bohagen, P. Orten, and G. E. Oien, “Construction and capacity analysis of high-rank line-of-sight MIMO channels,” *IEEE Wireless Communications and Networking Conference*, vol.1, pp. 432-437, March 13-17, 2005.

[13] N. Costa, S. Haykin, *Multiple-Input, Multiple-Output Channel Models Theory and Practice*, 1st ed., New York: John Wiley and Sons, 2009.

[14] D. Tse, P. Viswanath, *Fundamentals of Wireless Communication*, Cambridge Univ. Press, 2005.

[15] C. Sheldon et al., “Four-Channel Spatial Multiplexing Over a Millimeter-Wave Line-of-Sigh Link”, *IEEE Microwave Theory and Techniques Symposium*, pp. 389 - 392, Boston, MA, June 7-12, 2009.

[16] K. Leong, T. Itoh, “Advanced and Intelligent RF Front-End Technology”, *Wireless Communication Technology*, Conference Proceedings, pp.190 - 193, October 15 - 17, 2003.

[17] R. Feger, C. Wagner, S. Schuster, S. Scheiblhofer, H. Jager, A. Stelzer, “A 77-GHz FMCW MIMO Radar Based on an SiGe Single-chip Transceiver”, *IEEE Transactions on Microwave Theory and Techniques*, vol.57, no.5, pp. 1020 - 1035, May 2009.

[18] S.O. Tatu, E. Moldovan, S. Affes, “Low-cost Transceiver Architectures for 60 GHz UWB WLANs”, *International Journal of Digital Media Broadcasting*, ID 382695, 6 pp., April 2009.

[19] S.O. Tatu, E. Moldovan, S. Affes, “Multi-Port Front-End and Transceivers for V-Band Multi-Gigabit/s Communication Systems”, *Digital Front End*, chapter 24, Cambridge University Press,Cambridge, UK, September 2011, to appear.

[20] E. Moldovan, S.O. Tatu, S. Affes, Ke Wu, R. G. Bosisio, "W-band Substrate Integrated Waveguide Radar Sensor Based on Multi-port Technology", *4th European Radar Conference, European Microwave Week,* Conference Proceedings, pp. 174 - 177, Munich, October 8 - 12, 2007.

[21] B. N. Das, K. V. S. V. R. Prasad, and K. V. Seshagiri Rao, "Excitation of waveguide by stripline and microstrip-line-fed slots," IEEE Trans. Microwave Theory Tech., vol. MTT-34, pp. 321–327, Mar. 1986.

[22] W. Grabherr, B. Huder, and W. Menzel, "Microstrip to waveguide transition compatible with MM-wave integrated circuits," *IEEE Trans. Microwave Theory Tech.*, vol. 42, pp. 1842–1843, Sept. 1994.

[23] T. Q. Ho and Y. Shih, "Spectral-domain analysis of E-plane waveguide to microstrip transitions," *IEEE Transactions on Microwave Theory and Techniques*, vol. 37, pp. 388–392, Feb. 1989.

[24] L. J. Lavedan, "Design of waveguide-to-microstrip transitions specially suited to millimeter-wave applications," *Electron. Lett.*, vol. 13, Sept. 1977.

[25] Y. Cassivi, L. Perregrini, P. Arcioni, M. Bressan, K. Wu and G. Conciauro, "Dispersion Characteristics of Substrate Integrated Rectangular Waveguide," *IEEE Microwave and Wireless Comp. Lett.*, Vol. 12, Issue. 9, pp. 333- 335, Sept. 2002.

[26] Germain, S.; Deslandes, D.; Ke Wu, "Development of substrate integrated waveguide power dividers," *IEEE Canadian Conference on Electrical and Computer Engineering.* vol.3, pp.1921-1924, 4-7 May 2003

[27] Hammou, D.; Nedil, M.; Kandil, N.; Coulibaly, Y.; Moldovan, E.; Tatu, S.-O., "Microstrip to waveguide transition dedicated to wireless millimeter-wave applications, " *2012 IEEE Antennas and Propagation Society International Symposium (APSURSI),*pp.1,2, 8-14 July 2012

[28] A. Koelpin, G. Vinci, B. Laemmle, D. Kissinger, R. Weigel, "The Six-Port in Modern Society", *IEEE Microwave Magazine Supplement*, pp. 35 - 43, December 2010.

[29] S.O. Tatu, E. Moldovan, Ke Wu, R.G. Bosisio, T. Denidni, “Ka-Band Analog Front-end for Software Defined Direct Conversion Receiver”, *IEEE Transactions on Microwave Theory and Techniques*, vol.53, no.9, pp. 2768 - 2776, September 2005.

[30] S.O. Tatu, E. Moldovan, “V-band Multi-port Heterodyne Receiver for High-speed Communication Systems”, *EURASIP Journal on Wireless Comm. and Networking*, Article ID 34358, 7 pages, 2007.

[31] E. Moldovan, S. O. Tatu, “A 60 GHz Multi-Port Receiver with Analog Carrier Recovery for UWB WPAN”, *European Microwave Week*, pp. 1779 - 1782, Amsterdam, October 27 - 31, 2008.

[32] Ke Wu, S.O. Tatu, R.G. Bosisio, “Multi-port Interferometers for Ultra-wideband Transceiver Systems and Applications,” *2010 IEEE Microwave Theory and Techniques Symposium*, May 23, Anaheim, CA, 2010.

[33] Ji Li; Bosisio, R.G.; Ke Wu, “A six-port direct digital millimeter wave receiver,” *1994 IEEE National Telesystems Conference. Conference Proceedings.* pp.79-82, 26-28 May 1994.

[34] Tatu, S.-O.; Moldovan, E.; Ke Wu; Bosisio, R.G., “A new direct millimeter-wave six-port receiver,” *IEEE Transactions on Microwave Theory and Techniques,* , vol.49, no.12, pp.2517-2522, Dec 2001

[35] Moldovan, E.; Tatu, S.-O.; Gaman, T.; Ke Wu; Bosisio, R.G., “A new 94-GHz six-port collision-avoidance radar sensor,” *IEEE Transactions on Microwave Theory and Techniques*, vol.52, no.3, pp.751-759, March 2004

[36] Xinyu Xu; Bosisio, R.G.; Ke Wu, “Analysis and implementation of six-port software-defined radio receiver platform,” *IEEE Transactions on Microwave Theory and Techniques*, vol.54, no.7, pp.2937-2943, July 2006

[37] Chi-Hsueh Wang; Hong-Yeh Chang; Pei-Si Wu; Kun-You Lin; Tian-Wei Huang; Huei Wang; Chun Hsiung Chen, “A 60GHz Low-Power Six-Port Transceiver for Gigabit Software-Defined Transceiver Applications,” *IEEE International Solid-State Circuits Conference. Digest of Technical Papers.* , pp.192-596, 11-15 Feb. 2007

[38] D. Hammou, E. Moldovan, S.O. Tatu, “Novel MHMIC Millimeter Wave Power Divider/Combiner”, accepted to *2011 IEEE Canadian Conference on Electrical and Computer Engineering (CCECE 2011)*, Niagara Falls, Ontario, May 8 - 11, 2011.

[39] G. F. Engen, “The six-port reflectometer. An alternative network analyzer,” *IEEE Transactions on Microwave Theory and Techniques*, vol. 25, No. 12, 1075-1080, 1977.

[40] Li-Han Hsu et al., “Flip-Chip-Based Multichip Module for Low Phase-Noise V-Band Frequency Generation”, *IEEE Transactions on Microwave Theory and Techniques*, vol.58, no.9, pp. 2408 - 2419, September 2010.

[41] S.O. Tatu, B. Boukari, E. Moldovan, Ke Wu, R. G. Bosisio, “Millimeter Wave Multi-Port Radar Sensor with Integrated Receiver Front-end for Automotive Applications”, submitted to *IEEE Transactions on Microwave Theory and Techniques (MTT)*, Mars 2011.

[42] K. Ohata, K. Maruhashi, M. Ito, S. Kishimoto, K. Ikuina, T. Hashiguchi, K. Ikeda, and N. Takahashi, “1.25 gbps wireless gigabit ethernet link at 60ghz-band,” in *2003 IEEE MTT-S International Microwave Symposium Digest*, vol. 1, June 2003, pp. 373–376.

[43] Fujii, K.; Adamski, M.; Bianco, P.; Gunyan, D.; Hall, J.; Kishimura, R.; Lesko, C.; Schefer, M.; Hessel, S.; Morkner, H.; Niedzwiecki, A., "A 60 GHz MMIC chipset for 1-Gbit/s wireless links," *2002 IEEE MTT-S International Microwave Symposium Digest*, pp.1725-1728 vol.3, 2-7 June 2002

[44] Siligaris, A.; Chaix, F.; Pelissier, M.; Puyal, V.; Zevallos, J.; Dussopt, L.; Vincent, P., "A low power 60-GHz 2.2-Gbps UWB transceiver with integrated antennas for short range communications," *2013 IEEE Radio Frequency Integrated Circuits Symposium (RFIC)*, pp.297-300, 2-4 June 2013

[45] A. Tomkins et al., “A zero-IF 60 GHz transceiver in 65 nm CMOS with 3.5 Gb/s links,”, *IEEE Custom Integrated Circuits Conference*, pp. 471 - 474, San Jose, September 21 - 24, 2008.

[46] C. H. Wang et al., “A 60 GHz Low-Power Six-Port Transceiver for Gigabit Software-Defined Transceiver Applications,” *IEEE Solid-State Circuits Conference*, pp.192 - 196, Feb. 11 - 15, 2007.

[47] H. Wang, “Current status and future trends for Si and compound MMICs in millimeter-wave regime and related issues for system on chip (SOC) and/or system in package (SIP) applications”, *2010 Topical Meeting on Silicon Monolithic Integrated Circuits in RF Systems* (*SiRF*), D.O.I. 10.1109/SMIC.2010.5422975, pp. 1-16, New Orleans, January 11- 13, 2010.

[48] J. Laskar et al. “60 GHz Entertainment Connectivity Solution”, *IEEE International Conference on Ultra-Wideband*, pp. 17 -21, Vancouver, September 9 - 11, 2009.

[49] Mahmouli, F.E.; Walker, S.D., “4-Gbps Uncompressed Video Transmission over a 60-GHz Orbital Angular Momentum Wireless Channel,” *IEEE Wireless Communications Letters*, vol.2, no.2, pp.223-226, April 2013

[50] Katayama, Y.; Haymes, C.; Nakano, D.; Beukema, T.; Floyd, B.; Reynolds, S.; Pfeiffer, U.; Gaucher, B.; Schleupen, K., “2-Gbps Uncompressed HDTV Transmission over 60-GHz SiGe Radio Link,” *4th IEEE Consumer Communications and Networking Conference.* pp.12-16, Jan. 2007

[51] J.F. Frigon, B. Daneshrad, “A Multiple Input-Multiple Output (MIMO) Adaptive Decision Feedback Equalizer (DFE) with Cancellation for Wideband Space-Time Communications,” *International Journal of Wireless Information Networks*, vol. 9, no. 1, pp. 13 - 23, Jan. 2002.

[52] W. Ajib, D. Haccoun, J.F. Frigon, “Analysis and Evaluation of Link Layer Transmission Schemes for MIMO Channels,” *IEEE Trans. on Vehicular Techn.*, vol. 57, no. 3, pp. 1923 - 1929, May 2008.

[53] Ben Mabrouk, I.; Hautcoeur, J.; Talbi, L.; Nedil, M.; Hettak, K., “Feasibility of a Millimeter-Wave MIMO System for Short-Range Wireless Communications in an Underground Gold Mine,” *IEEE Transactions on Antennas and Propagation,* , vol.61, no.8, pp.4296-4305, Aug. 2013

[54] Sheldon, C.; Torkildson, E.; Munkyo Seo; Yue, C.P.; Rodwell, M.; Madhow, U., “Spatial multiplexing over a line-of-sight millimeter-wave MIMO link: A two-channel hardware demonstration at 1.2Gbps over 41m range,” *European Conference on Wireless Technology*. pp.198-201, 27-28 Oct. 2008

[55] U. Madhow, “Multi-Gigabit Millimeter Wave Communication: System Concepts and Challenges”, *Information Theory and Applications Ws.*, pp. 193 - 196, San Diego, January 27 - February 2, 2008.

[56] Jiang, T.; Hammou, D.; Hannachi, C.; Nedil, M.; Frigon, J.-F.; Wu, K.; Tatu, S.O., “Six-port technology for millimeter wave MIMO systems,” *2013 European Microwave Conference (EuMC)*, pp.1591-1594, 6-10 Oct. 2013

[57] E. Torkildson, C. Sheldon, U. Madhow, M. Rodwell, “Millimeter Wave Spatial Multiplexing in an Indoor Environment”, *IEEE Globecom Ws.* pp. 1 - 6, Honolulu, November 30 – December 4, 2009.

[58] Palaskas, Y.; Ravi, A.; Pellerano, S.; Carlton, B.R.; Elmala, M.A.; Bishop, R.; Banerjee, G.; Nicholls, R.B.; Ling, S.K.; Dinur, N.; Taylor, S.S.; Soumyanath, K., “A 5-GHz 108-Mb/s 2 × 2 MIMO Transceiver RFIC With Fully Integrated 20.5-dBm P_{1dB} Power Amplifiers in 90-nm CMOS,” *IEEE Journal of Solid-State Circuits*, vol.41, no.12, pp.2746-2756, Dec. 2006

[59] E. Torkildson, Hong Zhang, and U. Madhow, “Channel modeling for millimeter wave MIMO,” *Information Theory and Applications Workshop* (ITA), pp. 1-8, Jan. 31-Feb. 5, 2010.

[60] E. Torkildson, B. Ananthasubramaniam, U. Madhow, and M. Rodwell, “Millimeter-wave MIMO: Wireless Links at Optical Speeds,” Proceedings of 44th *Allerton Conference on Communication, Control and Computing*, 2006.

[61] A. Pollok, W. G. Cowley, I. D. Holland, “Multiple-Input Multiple-Output Options for 60 GHz Lineof- Sight Channels”, *Australian Comm. Theory Ws*, pp. 101 - 106, January 30 - February 1, 2008.

[62] S.J. Lee, M. G. Kyeong, W. Y. Lee, “Capacity Analysis of MIMO Channel with Line-of-Sight and Reflected Paths for Millimeter-Wave Communication”, *4th International Conference on Signal Processing and Communication Systems*, pp. 1 - 5, Gold Coast, Australia, December 13 - 15, 2010.

[63] S. Ranvier, J. Kivinen, P. Vainikainen, “Development of a 60 GHz MIMO Radio Channel Measurement System”, *Instrumentation and Measurement Technology Conference*, pp. 1878 - 1882, Ottawa, Canada, May 17 - 19, 2005.

[64] D. Hammou, N. Hakem, E. Moldovan, N. Khandil, and S.O. Tatu, “New V-band MHMIC Six-Port Architecture”, *9th IEEE International NEWCAS Conference*, pp. 422-425, Bordeaux, France, June 26-29, 2011.